Check for updates

JGR Biogeosciences

RESEARCH ARTICLE
10.1029/2024JG008650

Suppression of Methanogenesis by Microbial Reduction of Iron-Organic Carbon Associations in Fully Thawed Permafrost Soil

E. Voggenreiter[1], L. ThomasArrigo[2], M. Bottaro[1], J. Kilian[3], D. Straub[4], F. Ring-Hrubesh[5], C. Bryce[5], M. Stahl[3], A. Kappler[1,6], and P. Joshi[1]

[1]Department of Geosciences, Geomicrobiology, University Tuebingen, Tuebingen, Germany, [2]Environmental Chemistry, University of Neuchâtel, Neuchâtel, Switzerland, [3]Center for Plant Molecular Biology, University of Tuebingen, Tuebingen, Germany, [4]Quantitative Biology Center (QBiC), University of Tuebingen, Tuebingen, Germany, [5]School of Earth Sciences, University of Bristol, Bristol, UK, [6]Cluster of Excellence: EXC 2124: Controlling Microbes to Fight Infection, Tuebingen, Germany

Abstract Global methane (CH_4) emissions from thawing permafrost peatlands are expected to increase substantially in the future. Net emission of CH_4 depends on the presence of more favorable terminal electron acceptors for microbial respiration, such as ferric iron (Fe(III)). In soils with high OC content, Fe(III) is often coprecipitated with organic carbon (OC). The presence of Fe(III)-OC coprecipitates could either suppress CH_4 emissions due to inhibition of methanogenesis and stimulation of anaerobic methane oxidation coupled to Fe (III) reduction, or enhance emissions by providing additional OC. Here, we investigated the role of Fe(III)-OC coprecipitates in net CH_4 release in a fully thawed, waterlogged permafrost peatland (Stordalen Mire, Abisko, Sweden). We synthesized Fe(III)-OC coprecipitates using natural organic matter from the field site and added them to waterlogged soil in a microcosm experiment and in situ, and followed Fe speciation and changes in greenhouse gas emissions over time. Fe(III)-OC coprecipitates were partially reduced (22%) within 42 days in the microcosm experiment, while almost full reduction (92 ± 4%) occurred in situ within 53 days. This led to a decrease in CH_4 emissions by 94% and 40% in the microcosm and field experiments, respectively, compared to no-coprecipitate controls. A decrease in both RNA-based *mcrA* copy numbers and relative abundance of detected methanogens indicated that methanogenesis was mainly inhibited by the addition of the coprecipitates due to microbial Fe(III) reduction. In conclusion, Fe(III)-OC coprecipitates temporarily suppress net CH_4 emissions in fully thawed permafrost soils, and might play a similar role in mitigating CH_4 release in other (periodically) flooded soils.

Plain Language Summary Emissions of methane, a greenhouse gas 28 times more potent than carbon dioxide, are expected to increase globally. Most natural methane emissions originate from flooded soils, such as thawing permafrost soils. To better predict the future release of methane, it is important to understand the processes that result in its production and consumption. One of the key factors in net methane emission is the presence of other geochemical species such as iron-bearing phases that may be used by microorganisms for anaerobic respiration, potentially suppressing methane release. In this study, we investigated the role of previously overlooked iron-organic carbon associations in net methane emissions in a fully thawed permafrost soil. We found that iron-organic carbon associations were used by iron-reducing microorganisms which inhibited the activity of methane-producing microorganisms. This decreased the net methane emission from the soil by 94% and 40% in laboratory- and field-based experiments, respectively. Our findings therefore indicate that the presence of iron-organic carbon associations can temporarily decrease net methane emissions in thawing permafrost soil, and possibly in other flooded soils.

Key Points:

- Addition of iron(III)-organic carbon associations to fully thawed waterlogged permafrost soil decreases net methane release
- Methane emissions were mainly decreased by inhibition of methanogenesis and minor contributions of anaerobic methane oxidation
- Iron(III)-organic carbon associations may play a role in attenuating methane release in many (periodically) flooded soils

Supporting Information:

Supporting Information may be found in the online version of this article.

Correspondence to:

P. Joshi,
prachi.joshi@uni-tuebingen.de

Citation:

Voggenreiter, E., ThomasArrigo, L., Bottaro, M., Kilian, J., Straub, D., Ring-Hrubesh, F., et al. (2025). Suppression of methanogenesis by microbial reduction of iron-organic carbon associations in fully thawed permafrost soil. *Journal of Geophysical Research: Biogeosciences*, *130*, e2024JG008650. https://doi.org/10.1029/2024JG008650

Received 22 NOV 2024
Accepted 14 FEB 2025

Author Contributions:

Conceptualization: E. Voggenreiter, L. ThomasArrigo, A. Kappler, P. Joshi
Data curation: M. Bottaro, J. Kilian, D. Straub, F. Ring-Hrubesh, C. Bryce, M. Stahl
Formal analysis: E. Voggenreiter, L. ThomasArrigo, J. Kilian, D. Straub, F. Ring-Hrubesh, C. Bryce, M. Stahl, P. Joshi
Funding acquisition: A. Kappler
Investigation: E. Voggenreiter, L. ThomasArrigo, P. Joshi
Methodology: E. Voggenreiter, L. ThomasArrigo, M. Bottaro, J. Kilian,

© 2025. The Author(s).
This is an open access article under the terms of the Creative Commons Attribution License, which permits use, distribution and reproduction in any medium, provided the original work is properly cited.

1. Introduction

Methane (CH_4) is a potent greenhouse gas that is emitted globally at a rate of 576 Tg CH_4 y^{-1}, with a large portion (148 Tg y^{-1}) originating from periodically or permanently anoxic soils (Saunois et al., 2020). It is predicted that soil methane emissions will increase by 89% (SSP 2) until the year 2200 compared with 2010 (Kleinen et al., 2021). Permafrost peatlands will play an especially large role in CH_4 release in the future, since these soils contain a large organic carbon (OC) stock of which a substantial fraction represents labile, previously unavailable (frozen) OC (Lim et al., 2022; Mueller et al., 2015). In low-lying permafrost peatlands in which drainage of

21698961, 2025, 3, Downloaded from https://agupubs.onlinelibrary.wiley.com/doi/10.1029/2024JG008650 by Université de Neuchâtel, Wiley Online Library on [03/02/2026]. See the Terms and Conditions (https://onlinelibrary.wiley.com/terms-and-conditions) on Wiley Online Library for rules of use; OA articles are governed by the applicable Creative Commons License

D. Straub, F. Ring-Hrubesh, C. Bryce, M. Stahl, P. Joshi
Project administration: L. ThomasArrigo, P. Joshi
Supervision: L. ThomasArrigo, A. Kappler, P. Joshi
Visualization: E. Voggenreiter
Writing – original draft: E. Voggenreiter
Writing – review & editing: L. ThomasArrigo, J. Kilian, D. Straub, F. Ring-Hrubesh, C. Bryce, A. Kappler, P. Joshi

thawed permafrost is impeded or which are hydrologically connected to other water bodies, soil inundation and thermokarst formation is predicted (Farquharson et al., 2019; Kokelj & Jorgenson, 2013; Varner et al., 2022; Woo & Young, 2006). As these soils are saturated with water, anoxic conditions are expected to develop and may lead to increasing CH_4 emissions, promoted further by increasing temperatures (Knoblauch et al., 2018; Rößger et al., 2022; Turetsky et al., 2008). The net release of CH_4 depends on the balance of CH_4 production by methanogens and CH_4 oxidation by methanotrophs (Bridgham et al., 2013), which are affected by varying biogeochemical parameters. The key parameter in this release is the availability of terminal electron acceptors that are more thermodynamically favorable than CO_2, such as nitrate, sulfate, or ferric iron (Fe(III)) minerals (Achtnich et al., 1995; Stams et al., 2003).

The net effect of the presence of Fe(III) minerals on CH_4 release can vary. First, many studies reported inhibition of methanogenesis when Fe(III) reduction occurred (Lipson et al., 2012; Miller et al., 2015; Reiche et al., 2008; Roden & Wetzel, 1996). The main reason for inhibition is that Fe(III) reduction outcompetes methanogenesis thermodynamically, implying that methanogenesis will proceed only once Fe(III) is depleted (Bridgham et al., 2013; Megonigal et al., 2003). Second, Fe(III)-reducing microorganisms and methanogens compete for the same substrates, such as acetate and hydrogen (H_2), which Fe(III)-reducers can use at far lower concentrations than methanogens (Roden & Wetzel, 2003). Fe(III) might also play a role within anaerobic oxidation of CH_4 by functioning as an electron acceptor (Bar-Or et al., 2017; Ettwig et al., 2016), thus decreasing net CH_4 release. In contrast, there is also evidence that Fe(III) reduction can promote methanogenesis. One theoretical argument is that the pH increase induced by Fe(III) reduction could make conditions more favorable for (acetoclastic) methanogenesis (Sulman et al., 2022; Wagner et al., 2017). Additionally, there is evidence from culture-based (Fu et al., 2019; H. Wang et al., 2020) and soil-based (Xiao et al., 2019) studies that more crystalline Fe(III) minerals can serve as electron shuttles for methanogens.

In contrast to pure Fe(III) minerals and dissolved Fe(III), much less is known about the influence of organic matter-bound Fe(III) on net CH_4 release. Poorly crystalline, high surface area Fe(III) minerals, such as ferrihydrite, are often associated with organic matter through adsorption or coprecipitation (Dong et al., 2023), forming Fe(III)-OC associations. In permafrost peatland soils with high OC content, binding through coprecipitation is thought to be the dominant process based on OC:Fe ratios of selective extractions (Patzner et al., 2020; Sun et al., 2023; Y. Wang et al., 2022). Fe(III)-OC coprecipitates may play an inhibitory or promotive role regarding CH_4 release. Once conditions turn anoxic, Fe(III) reduction may occur, releasing Fe^{2+} and the previously bound OC to the aqueous phase. Since Fe(III)-OC coprecipitates are less crystalline than OC-free Fe(III) minerals, they might be more available for microbial reduction (Adhikari et al., 2017; Cooper et al., 2017) and lead to stronger suppression of methanogenesis. On the other hand, the released OC could function as a substrate for fermenting microorganisms, providing more substrates for methanogenesis (fatty acids, H_2) (Drake et al., 2009). High OC loadings in Fe(III)-OC coprecipitates could also inhibit microbial access to Fe (Eusterhues et al., 2014), decreasing the extent of Fe(III) reduction and thus the competition with methanogenesis. The C and Fe cycles in anoxic soils are thus closely interlinked through the processes of Fe(III) reduction, fermentation, and methanogenesis.

Thawing permafrost soils provide a suitable ecosystem to study this linkage. An increasing number of studies reported that Fe-bound OC accounts for a significant fraction of total soil OC (up to 20%) in intact permafrost (Liu et al., 2022; Mu et al., 2016; Patzner et al., 2020). At the onset of thaw, these Fe(III)-OC associations are (partially) reductively dissolved. Often, CH_4 emissions are detected simultaneously (Lipson et al., 2012; Monhonval et al., 2022; Patzner, Logan, et al., 2022). However, the role of Fe(III)-OC associations in net CH_4 release is still unclear. Current knowledge based on field observations only provides correlations between Fe cycling and CH_4 release, but direct experimental evidence is lacking. Therefore, the objectives of this study were (a) to determine the reduction extent of Fe(III)-OC associations over several weeks in a fully thawed permafrost soil, (b) to quantify the net effect of Fe(III) reduction of Fe(III)-OC associations on CH_4 release, and (c) to identify main microbial groups relevant to CH_4 cycling due to addition of Fe(III)-OC associations. To achieve this, we incubated synthesized Fe(III)-OC coprecipitates together with soil from a fully thawed permafrost peatland (Stordalen Mire, Abisko, Sweden) within a microcosm experiment and an in situ field experiment. In the microcosm experiment, we aimed to gain a mechanistic understanding of the processes underlying CH_4 release with Fe(III)-OC coprecipitate addition. Within the field experiment, our aim was to estimate the overall net effect of Fe(III)-OC coprecipitate addition on CH_4 release under relevant environmental conditions. We used a combination of isotope-specific techniques as well as spectroscopic and molecular biology methods to track the reduction of Fe

21698961, 2025, 3, Downloaded from https://agupubs.onlinelibrary.wiley.com/doi/10.1029/2024JG008650 by Université de Neuchâtel, Wiley Online Library on [03/02/2026]. See the Terms and Conditions (https://onlinelibrary.wiley.com/terms-and-conditions) on Wiley Online Library for rules of use; OA articles are governed by the applicable Creative Commons License

(III)-OC coprecipitates, emission of CH_4 and carbon dioxide (CO_2), and changes in the abundance and activity of relevant methane-cycling microorganisms.

2. Materials and Methods

2.1. Field Site Description and Sampling

Stordalen Mire is a thawing permafrost peatland, located near Abisko, Sweden (68 22′N, 19 03′E). It is situated in the discontinuous permafrost zone and consists of intact permafrost areas (palsa hills), covered by dwarf shrubs, bryophytes and lichens (52% of areal cover), semi-wet bogs dominated by *Sphagnum ssp.* mosses (32% areal cover), and fully inundated fens covered by sedges, such as *Eriophorum vaginatum* and *Carex rostrata* (16% areal cover) (Malmer et al., 2005; Varner et al., 2022).

The fen soil was sampled in July 2022 at two depths that differed in organic matter content. The upper organic-rich soil (38% soil OC) was sampled from 2 to 10 cm depth below the soil surface and used to extract soil organic matter for synthesis of (^{57}Fe-enriched) Fe(III)-OC coprecipitates (see 2.2). The organic-poor (2.5% soil OC), mineral-rich soil was sampled at 30 cm depth and used for the lab-based microcosm experiment. The soils were collected by grab sampling and stored in sterilized plastic bags (LDPE). Both layers were water saturated and the soil was filled into the bags so that no headspace was remaining. Soils were stored at 4°C after collection and kept under cool conditions during transport. Back in Tübingen, the soils were stored in gas-tight, N_2-flushed mason jars at 4°C until use. A subsample of the mineral soil was dried inside an anoxic glovebox (MBraun Unilab Workstation, 100% N_2 atmosphere) at 60°C for general soil characterization. We determined the mineralogy by X-ray diffractometry (XRD), soil OC content by elemental analysis, and total Fe content by X-ray fluorescence (XRF) as well as Fe speciation by Fe *K*-edge X-ray absorption spectroscopy (XAS). More details are given in Text S1 in Supporting Information S1. Fe content and speciation in poorly crystalline and highly crystalline Fe pools were analyzed after anoxic 0.5 and 6 M HCl extractions (Figure S1 in Supporting Information S1).

2.2. Synthesis of (^{57}Fe-Enriched) Fe(III)-OC Coprecipitates

To synthesize Fe(III)-OC coprecipitates, soil organic matter from the fen organic horizon was extracted. Field-moist soil was added to double-deionized water (DDI, Millipore, >18 MΩ cm^{-1}) at a 1:10 weight/volume (w/v) ratio for 24 hr on an overhead shaker in the dark. Afterwards, the suspensions were centrifuged in pre-baked glass serum bottles (5,250 rcf, 15 min) and the supernatant was sequentially filtered through pre-rinsed 8 µm (Merck Millipore, MCE) and 0.22 µm (Merck Millipore, Steritop PES) filters. The resulting water-extractable organic matter (WEOM) was stored at 4°C for less than 24 hr until use. The dissolved organic carbon (DOC) concentration was 24 mg C L^{-1}.

The coprecipitates used in the microcosm experiment were prepared from a ^{57}Fe-enriched (10%) $FeCl_3$ solution (details in Text S2 in Supporting Information S1), which enabled a differentiation of the added Fe minerals from the native Fe pool and improved the analysis by ^{57}Fe-specific Mössbauer spectroscopy. Both ^{NA}Fe- and ^{57}Fe-enriched Fe(III)-OC coprecipitates were synthesized by mixing 1.5 L of WEOM with 20 mL of the respective $FeCl_3$ solution (initial C:Fe ratio = 1), after which NaOH solution was added until pH 6. The final suspension was bubbled with N_2 (99.999%) for 15 min to make it anoxic. Fe speciation was analyzed by the ferrozine assay (Stookey, 1970) after dissolution in 1 M HCl, and mineral identity was determined by ^{57}Fe Mössbauer spectroscopy (Figure S2 in Supporting Information S1) and Fe *K*-edge XAS (Figure S3 in Supporting Information S1).

2.3. Microcosm Experiment to Elucidate the Net Effect of Fe(III)-OC Coprecipitate Addition on Greenhouse Gas Fluxes

2.3.1. Setup of Microcosm Experiment

For the microcosm experiment, we used the mineral subsoil for two reasons. First, it represents end-state conditions of permafrost thaw and has thus undergone thaw-related geomicrobiological changes. Second, most native Fe(III)-OC associations are contained in this soil layer. Prior to using the mineral soil, it was homogenized by wet sieving under oxic conditions with a sterilized 2 mm sieve. Subsequently, field moist soil (12 g dry weight) was added to six 250 mL serum bottles under sterile conditions. The bottles were closed with sterilized butyl rubber stoppers and crimped with aluminum caps. The headspace in the bottles was exchanged by applying vacuum for 5 min and flushing with N_2 gas for 5 min (3 cycles). These six bottles were later split up into two sets of triplicates,

21698961, 2025, 3, Downloaded from https://agupubs.onlinelibrary.wiley.com/doi/10.1029/2024JG008650 by Université de Neuchâtel, Wiley Online Library on [03/02/2026]. See the Terms and Conditions (https://onlinelibrary.wiley.com/terms-and-conditions) on Wiley Online Library for rules of use; OA articles are governed by the applicable Creative Commons License

one set which was amended with ^{57}Fe-enriched Fe(III)-OC coprecipitates and one set functioning as a non-amended control. The bottles were transferred to an anoxic glovebox and sterile, anoxic, artificial porewater solution (composition in Table S1 in Supporting Information S1) was added: 135 mL for control treatments and 100 mL for coprecipitate-added treatments, to reach a final ratio of 85 mg dry soil mL^{-1} for both treatments. All bottles were incubated under anoxic conditions at room temperature in the dark for 35 days prior to the addition of ^{57}Fe-enriched Fe(III)-OC coprecipitates. This initial incubation served to establish anoxic conditions in the soil, to avoid the first pulse of greenhouse gases due to rewetting (Kim et al., 2012), and to reduce all easily reduceable native Fe(III) minerals. Geochemical sampling was done once each week to monitor Fe(III) reduction (see below). The amount of added synthesized ^{57}Fe-enriched coprecipitates constituted an increase in total 6 M HCl-extractable Fe by 50% (4.17 mg Fe g^{-1} dry soil, Figure S4d in Supporting Information S1).

To test the occurrence of abiotic isotopic exchange between aqueous $^{56}Fe^{2+}$ and ^{57}Fe(III) in coprecipitates, we performed an additional control experiment. We added the same concentration of Fe(III)-OC coprecipitates to filtered (0.22 μm, PES, Carl Roth) solution from the control microcosms. The Fe(III)-OC coprecipitates were prepared as a new batch in order to have the same storage time as for the main experiment. The filtered porewater was diluted to have the same DOC concentration as on t_0 of the main experiment. The aqueous Fe concentration and speciation as well as fraction of ^{57}Fe was then quantified over 48 hr.

2.3.2. Sampling of Microcosm Experiment

Analysis of the microcosms included measuring greenhouse gas (GHG) fluxes and sampling for geochemical changes. To measure GHG fluxes, the rubber stopper of each bottle was pierced with 2 needles, each with a three-way valve attached. After 10 min of flushing the bottles with moistened N_2 gas, the N_2 flow was stopped, the overpressure was released into water via a tube, and the gases were left to accumulate for 60 min. A 2 mL sample was taken from the headspace and transferred to a He-flushed 12 mL Exetainer® vial (Labco, UK) after 0, 30, and 60 min. The flux incubation time was increased to 90 min after 32 days of the incubation to detect a sufficient GHG concentration increase. The sampling volume relative to the headspace volume of the bottles was <5%. The individual and cumulative gas fluxes were calculated based on the increase in gas concentration, given in Text S4 in Supporting Information S1.

The bottles were then transferred to the glovebox for geochemical sampling. An aliquot of the suspension (1 mL before coprecipitate addition, 1.5 mL afterward) was taken. The sample was centrifuged (10,055 rcf, 5 min) and the supernatant was collected. The supernatant was used to quantify DOC concentration and aqueous Fe speciation after acidification with anoxic 1 M HCl. The soil pellet was dried at 60°C anoxically overnight and weighed to estimate the dry mass in each sample. To target the poorly crystalline Fe mineral fraction, 1.5 mL anoxic 0.5 M HCl was added and left to equilibrate with the soil for 24 hr (Heron et al., 1994; Kostka & Luther, 1994). The extraction solution and remaining solid were separated by centrifugation (10,055 rcf, 5 min) and the supernatant was diluted in 1 M HCl for analysis of Fe speciation and ^{57}Fe concentration. At certain time points (right after addition of coprecipitates, after 8, 15, and 42 days) an additional 15 mL of suspension was taken from the bottles. An aliquot (4 mL) was centrifuged in the glovebox, the supernatant was transferred to a new tube and immediately frozen (−20°C) for measurement of microbial metabolites by gas chromatography mass spectrometry (GC-MS). The soil pellet was frozen (−20°C) and subsequently freeze-dried under anoxic conditions for analysis by ^{57}Fe Mössbauer spectroscopy. An aliquot of 1 mL was used to measure pH (InLab Easy BNC, Mettler Toledo, Germany) outside the glovebox. The remaining 10 mL were transferred to 15 mL centrifuge tubes (polypropylene, RNase- and DNase-free, Biologix) and centrifuged outside the glovebox (17,200 rcf, 5 min). The supernatant was taken off under sterile conditions and the remaining soil pellet was immediately frozen (−80°C) for later extraction of DNA and RNA and subsequent molecular biological analysis (see Section 2.3.5).

2.3.3. Geochemical Analyses

Aqueous and solid (0.5 M HCl-extractable) Fe speciation and total Fe concentration were quantified using the ferrozine assay (Stookey, 1970). DOC concentration was measured (as non-purgeable OC) after acidification with 2 M HCl by a TOC analyzer (multi N/C 2100S, Analytik Jena AG, Germany). A gas chromatograph (TraceGC1300, ThermoFisher Scientific, USA; modified by S + HA analytics) was used to measure GHG concentrations. It was equipped with an autosampler and 2 column configurations (first configuration: 30 m long,

21698961, 2025, 3, Downloaded from https://agupubs.onlinelibrary.wiley.com/doi/10.1029/2024JG008650 by Université de Neuchâtel, Wiley Online Library on [03/02/2026]. See the Terms and Conditions (https://onlinelibrary.wiley.com/terms-and-conditions) on Wiley Online Library for rules of use; OA articles are governed by the applicable Creative Commons License

0.53 mm ID TGBondQ column and 30 m long, 0.53 mm ID Molsieve column; second configuration: 30 m long, 0.53 mm ID TGBondQ column and a 30 m long 0.25 mm ID TGBondQ + column; all ThermoFisher Scientific) which are each connected to a Pulse Discharged Detector. Concentrations of CH_4, N_2O, and CO_2 were quantified with calibrations of standards using pure gases (99.5% CH_4, 99.9% CO_2, 99.999% N_2O, Westfalen, Germany) in He-flushed Exetainer® vials in a range of 0.05–500 ppm. N_2O was always below detection limit in the microcosm experiment and did not significantly increase during measurements in the field experiment. Concentrations of ^{57}Fe in aqueous and 0.5 M HCl-extracted solid samples were quantified by inductively coupled plasma mass spectrometry (ICP-MS, Agilent 7900, Agilent Technologies, USA) with Ar as carrier gas and in He mode after dilution in 1% HNO_3 (analytical grade, Carl Roth). Contribution of ^{57}Fe-enriched Fe(III)-OC coprecipitates to the aqueous and solid (0.5 M HCl-extractable) Fe pool were calculated (Text S5 in Supporting Information S1) and raw data (f(^{57}Fe)) are given in Figure S4 in Supporting Information S1.

2.3.4. Solid Phase Fe Characterization

^{57}Fe Mössbauer spectroscopy was used to analyze Fe speciation of the initial synthesized ^{57}Fe-enriched coprecipitates and in the solids from the microcosm experiment. Initial coprecipitates were collected by filtration (0.45 µm, nitrocellulose, Millipore). The filter paper with solids was fixed between Kapton® tape and frozen (−20°C). Anoxically freeze-dried samples from the microcosms (after centrifugation, as specified in Section 2.3.2 above) were ground with mortar and pestle in a glovebox and 60–80 mg were placed in 1 cm^2 Plexiglas holders. Samples at the beginning and end of the incubation were selected for analysis. Due to the enrichment of ^{57}Fe in the Fe(III)-OC coprecipitates, 51% of the signal within the Mössbauer spectra of the coprecipitate-added treatment originated from the coprecipitates (see calculation in Text S10 in Supporting Information S1), while the theoretical fraction of coprecipitate Fe in the total soil Fe was 17%. Samples were inserted into a closed-cycle exchange gas cryostat (Janis cryogenics) under a gasflow of He to minimize air exposure (see Text S6 in Supporting Information S1). Spectra were collected at 30 and 6 K for initial ^{57}Fe-enriched Fe(III)-OC coprecipitates and at 77 and 6 K for microcosm samples.

Iron speciation of the initial soil and synthesized ^{57}Fe-enriched coprecipitates was also investigated by Fe *K*-edge XAS at Synchrotron SOLEIL (SAMBA beamline, Paris, France). Oxidation state of Fe was determined by fitting of the Fe *K*-edge X-ray absorption near edge structure (XANES) while fitting of the extended X-ray absorption fine structure (EXAFS) was used to determine the Fe speciation. For this purpose, the initial ^{57}Fe-enriched coprecipitates were air-dried prior to homogenization with a mortar and pestle. The dried solids were each pressed into pellets (7 mm diameter) with PVP (Polyvinylpyrrolidone K12, Carl Roth), before being sealed with Kapton® tape. More details on synchrotron spectra acquisition and data analysis can be found in Text S6 in Supporting Information S1.

2.3.5. Molecular Biology Analysis

Total DNA and RNA of soil samples from the microcosm experiment were extracted in experimental triplicate using the RNeasy PowerSoil® Total RNA Kit with DNA Elution (Qiagen, Germany). Details on protocol adjustments and quality controls are listed in Text S7 in Supporting Information S1. Remaining DNA in the RNA samples was digested and the RNA was reverse transcribed using commercial kits (Invitrogen, Life Technologies, USA) as described in Otte et al. (2018). Bacterial and archeal 16S rRNA (gene) amplicon sequencing on both DNA and cDNA samples was done using the universal primers 515f (Parada et al., 2016) and 806r (Apprill et al., 2015) fused to Illumina adapters. Library preparation steps (Nextera, Illumina) and sequencing were performed using Illumina MiSeq sequencing system (Illumina, USA) at the Institute for Medical Microbiology and Hygiene of the University of Tübingen. Data processing, including quality control, reconstruction of sequences, and taxonomic annotation (Text S7 in Supporting Information S1) was done using nf-core/ampliseq version 2.8.0 (Straub et al., 2020, 2024) of the nf-core collection of workflows (Ewels et al., 2020). Methanogenic, methanotrophic, and Fe(III)-reducing taxa were identified, as listed elsewhere (Patzner, Kainz, et al., 2022, Patzner, Logan, et al., 2022) and references therein).

Quantitative PCR (qPCR) was performed on DNA and cDNA samples to quantify changes in total bacterial and archeal 16S rRNA (gene) copies and in functional genes relevant for CH_4 cycling. Specifically, we targeted the methyl-coenzyme M reductase subunit alpha (*mcrA*) gene, used as a marker gene for methanogens (Friedrich, 2005; Juottonen et al., 2006), and particulate methane monooxygenase (*pmoA*) gene, used to assess the

21698961, 2025, 3, Downloaded from https://agupubs.onlinelibrary.wiley.com/doi/10.1029/2024JG008650 by Université de Neuchâtel, Wiley Online Library on [03/02/2026]. See the Terms and Conditions (https://onlinelibrary.wiley.com/terms-and-conditions) on Wiley Online Library for rules of use; OA articles are governed by the applicable Creative Commons License

abundance of methanotrophs (McDonald et al., 2008; Welte et al., 2016). The used primer sequences, plasmid standards, dilution factors of samples, and details of the temperature programs are given in Table S2 in Supporting Information S1. The assays were performed using SybrGreen® Supermix (Bio-Rad Laboratories, USA) on the C1000 Touch thermal cycler (CFX96TM real time system, Bio-Rad Laboratories). Sample dilutions (10-1000x) were necessary since the presence of complex OC compounds led to inhibition of the fluorescence signal in samples without dilution (Winkel et al., 2018). Appropriate sample dilutions were tested (see Figure S5 in Supporting Information S1). Copy numbers were determined in analytical triplicates of each experimental replicate. Data analysis was performed in Bio-Rad CFX Maestro 1.1 software, versus 4.1 (Bio-Rad, 2017).

2.3.6. Analysis of Microbial Metabolites

The concentration of microbial metabolites, including small sugars, organic acids, and amino acids were quantified using targeted GC-MS (Shimadzu GC/MS TQ 8040, Japan). Some of the selected metabolites are important substrates or products of methanogenesis (acetate, methanol), Fe(III) reduction, or fermentation pathways (lactate, pyruvate). A full list of measured metabolites is given in Table S3 in Supporting Information S1. Metabolites were measured either by headspace injection or as liquid samples after derivatization and addition of octanole or ^{13}C-glucose as internal standard, respectively. More details are given in Text S8 in Supporting Information S1. Concentrations were quantified with a 8-point external calibration containing standards of all targeted analytes, ranging from 20 to max. 10^7 pmol.

2.4. Field Experiment to Determine In Situ Effect of Fe(III)-OC Coprecipitates on Greenhouse Gas Fluxes in Fully Thawed Fens

2.4.1. Construction of Peepers and Experiment Treatment

We performed a field experiment to determine the in situ reduction extent of ^{NA}Fe(III)-OC coprecipitates and the effect on net soil greenhouse gas emissions over a summer season. For this purpose, passive porewater samplers ("peepers", 20 cm length, 10 × 1 cm high cells, each of 12 mL volume) were constructed in house according to Bowes and Hornibrook (2006) after Hesslein (1976). Peepers are traditionally used to passively sample the aqueous phase in waterlogged soils or sediments (Hesslein, 1976; Lei et al., 2024), whereas here we employed them to incubate solids (^{NA}Fe(III)-OC coprecipitates) in the peeper cells. The coprecipitates were in contact with the soil over the subarctic summer period in the fen area at Stordalen Mire and could affect GHG emissions by suppressing methanogenesis and/or acting as a source of OC (as described in the introduction). A set of 3 peepers were inserted into the soil in July 2022 on plots with similar vegetation and ca. 1 m apart from each other. Cells of the peepers were filled with anoxic, deionized water through attached butyl rubber tubing prior to installation in the soil. The peepers were equilibrated for 4 days in the soil, after which an anoxic suspension of 280 mg Fe L^{-1} as ^{NA}Fe(III)-OC coprecipitates was added via the tubing to two of the peepers. The suspension was added into every second cell in the following depths from the soil surface: 4–5, 8–9, 12–13, 16–17, and 20–21 cm. The third peeper functioned as a control as only deionized water was added. Details on dimensions of the peepers and individual components are shown in Text S9 and Figure S6 in Supporting Information S1. We chose a membrane with 8 μm pore size in the peeper in order to facilitate microbial access to the ^{NA}Fe(III)-OC coprecipitates. It was also tested whether the ^{NA}Fe(III)-OC coprecipitates would pass the membrane in case of lower aggregate size. To test this, we placed the membrane inside filter cups (25 mm, Millipore) and filtered through 1 mL of initial coprecipitate suspension. The filtrate was acidified with 1 M HCl and total Fe concentration was measured as described in Section 2.3.3.

2.4.2. Sampling and Analysis of Field Experiment

Greenhouse gas emissions were determined above the peepers by placing static, non-flow gas chambers over them. Emissions were measured as described previously (Liebner et al., 2015), with the following adjustments: (a) the chambers were wrapped in aluminum foil to exclude photosynthetic processes, (b) incubation time was 20 min and samples were taken every 5 min by a gas-tight 50 mL syringe. Each gas sample (18 mL) was injected into pre-evacuated 12 mL Exetainer® vials. Gas fluxes were measured in triplicate in July (2, 20, and 21 hr after addition of coprecipitates) and then at the end of the summer season (September, after 53 days). One peeper containing the ^{NA}Fe(III)-OC coprecipitates ("+ cop") and one containing only deionized water ("– cop") were

21698961, 2025, 3, Downloaded from https://agupubs.onlinelibrary.wiley.com/doi/10.1029/2024JG008650 by Université de Neuchâtel, Wiley Online Library on [03/02/2026]. See the Terms and Conditions (https://onlinelibrary.wiley.com/terms-and-conditions) on Wiley Online Library for rules of use; OA articles are governed by the applicable Creative Commons License

selected for the gas measurements. Gas concentrations of CO_2 and CH_4 were measured as described in Section 2.3.3.

In order to assess the effect on porewater geochemistry and quantify the remaining ^{NA}Fe(III)-OC coprecipitate solids, we measured DOC, dissolved porewater gases (CO_2, CH_4) as well as dissolved and solid Fe concentrations after 53 days of incubation in September 2022. An N_2-filled 20 mL syringe was attached to one side of the butyl tubing of each cell, while another N_2-flushed, empty syringe was attached to the outlet side. The outlet-syringe was pulled to capture the anoxic solution in the peepers and the inlet syringe was simultaneously pushed to avoid underpressure and flow of new porewater into the peeper cell. The contents of the syringe were distributed in the following way: 7 mL were transferred to an N_2-flushed, gastight 50 mL serum vial and stored at 4°C until measurement of dissolved and solid Fe speciation. An aliquot of 3 mL was added to a He-filled 11 mL headspace vial to measure dissolved porewater gases. For that purpose, the vials were vigorously shaken for 2 min after which 3 mL of the headspace gas was transferred to a He-flushed, 12 mL Exetainer® vial. The remaining volume (1–2 mL) was filtered (0.22 µm, PES, Carl Roth; pre-rinsed with 50 mL DDI) and frozen (−20°C) until measurement of DOC.

Samples for measurement of aqueous and solid Fe speciation were prepared in an anoxic glovebox. An aliquot of 1 mL was filtered (0.22 µm, PES, Carl Roth) and stabilized with 1 mL of 2 M HCl to quantify aqueous Fe speciation. Total Fe in initial suspensions was determined by dissolving 0.8 mL unfiltered sample in 0.8 mL 2 M HCl. The solid Fe content and speciation was calculated by subtraction of aqueous from total concentrations. Analytical methods for determination of Fe speciation and concentration, dissolved porewater gases, and DOC concentration are described in Section 2.3.3.

2.5. Statistical Analyses

Mean and standard deviations were calculated for each parameter analyzed in triplicate. Differences in parameters between the two treatments (with Fe(III)-OC coprecipitate addition and the no-coprecipitate control) were calculated using the mean values and the errors were propagated. The following data sets were compared between the two treatments using a one-way ANOVA, followed by Tukey HSD tests: (a) the cumulative and individual greenhouse gas fluxes measured per time point in the microcosm and field experiments, (b) the relative abundances of detected methane-cycling microorganisms, (c) concentrations of microbial metabolites, and (d) absolute qPCR-based copy numbers. The relative abundance of all detected methanogens of the two treatments was compared using an unpaired *t*-test. A Kruskal-Wallis test was used in case of non-parametric data sets. All statistical analyses were performed in R version 4.3.3 (R Core Team, 2024).

3. Results and Discussion

3.1. Fe(III)-OC Coprecipitates Are Microbially Reduced in Microcosm Experiments

We assessed the reduction of Fe(III)-OC coprecipitates in the soil microcosm experiments based on aqueous and solid phase Fe data. Soil microcosms amended with ^{57}Fe-enriched Fe(III)-OC coprecipitates showed an increase in aqueous Fe^{2+} from 0.68 ± 0.02 mM directly after addition to 1.01 ± 0.02 mM after 42 days (Figure 1a), while the no-coprecipitate control had constant Fe^{2+} concentrations over time (0.72 ± 0.02 mM). This shows that there was more reductive dissolution of Fe(III) in the coprecipitate-added treatment than in the control. The difference in absolute aqueous Fe^{2+} concentrations between the two treatments would constitute a dissolution of 4.4 ± 0.4% of added coprecipitates. Based on the ^{57}Fe isotope data, 0.63 ± 0.01 mM Fe were reduced and released from coprecipitates (Figure 1b) within 42 days, confirming that this excess quantity of aqueous Fe^{2+} stemmed from the added ^{57}Fe-enriched Fe(III)-OC coprecipitates. The estimated net dissolution of added coprecipitates calculated from these isotopic data was higher (10.2 ± 0.2%) than based on absolute aqueous Fe^{2+} concentrations, possibly due to partial isotopic exchange (addressed below). In the solid phase, the Fe(II) to total Fe ratio (based on 0.5 M HCl extractions) increased from 46 ± 7% at t_0 to 70 ± 5% after 42 days for the coprecipitate-added treatment while it stayed constant in the no-coprecipitate control (88 ± 6%, Figure 1c). Both the aqueous phase Fe^{2+} data and the solid phase Fe(III) contents therefore show partial reduction of Fe(III)-OC coprecipitates. This reduction is likely microbial, based on higher CO_2 release in the coprecipitate-added treatment (shown in Section 3.3.) and supported by the presence of Fe(III)-reducing microorganisms such as *Geobacter* and *Rhodoferax* (Figure S7 in Supporting Information S1).

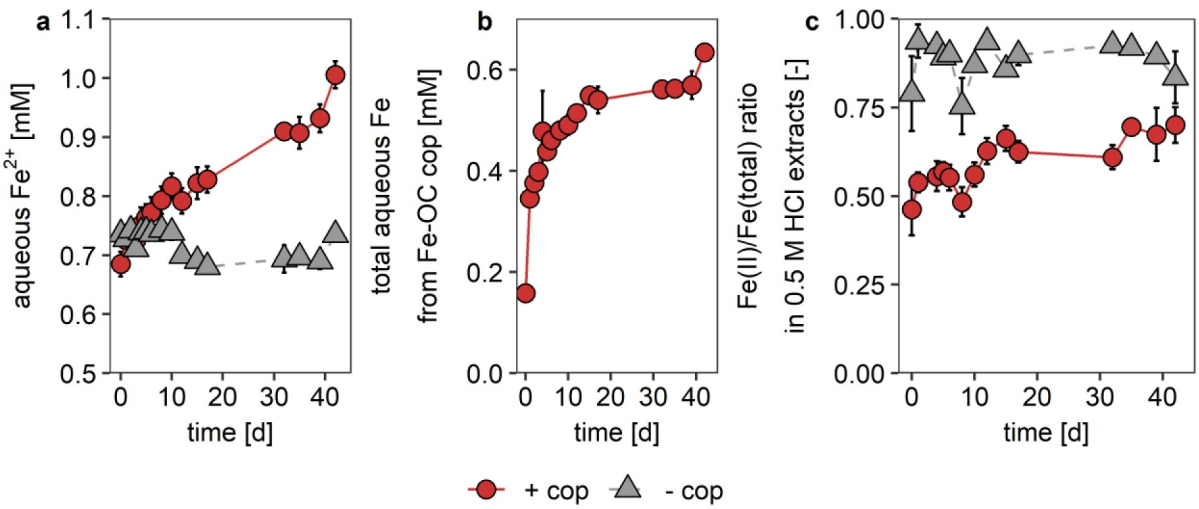

Figure 1. Changes in aqueous Fe and solid phase Fe speciation over time. Measured concentrations of dissolved Fe^{2+} in treatments with Fe(III)-OC coprecipitate addition ("+ cop", red circles) and the no-coprecipitate control ("− cop", gray triangles) (a). Calculated concentration of total aqueous Fe from Fe(III)-OC coprecipitates based on ^{57}Fe isotope measurements (b). Change in Fe(II) to total Fe(III) ratio of the 0.5 M HCl extracts for each treatment (c). All data symbols and error bars represent the average and standard deviation of experimental triplicates, respectively.

In a control experiment, we tested whether the changes in aqueous ^{57}Fe concentrations were influenced by abiotic isotope exchange of aqueous Fe^{2+} with the Fe in the added coprecipitates. This effect would have increased the fraction of ^{57}Fe in the aqueous phase by electron transfer from the aqueous $^{56}Fe^{2+}$ to the $^{57}Fe(III)$ in the coprecipitates and released $^{57}Fe^{2+}$ without any net reduction of coprecipitates taking place. Results showed rapid isotope exchange immediately after addition of Fe(III)-OC coprecipitates to the solution while absolute aqueous Fe concentrations stayed constant over 48 hr (Figure S8 in Supporting Information S1). The initial rapid increase in aqueous Fe from coprecipitates observed in our microcosms (0.35 mM after 1 day, Figure 1b) is therefore attributable to partial isotope exchange, while the remaining increase likely constitutes microbial Fe(III) reduction.

The extent of Fe(III) reduction and speciation of Fe phases (including those not captured by the 0.5 M HCl extraction) were analyzed using ^{57}Fe Mössbauer spectroscopy. We measured ^{57}Fe Mössbauer spectra of soil in both treatments at 77 and 6 K. Spectra at 6 K allowed for a more precise identification of Fe phases, while spectra at 77 K gave overall information on Fe speciation (see Figure S9, Text S11 in Supporting Information S1). In all 6 K spectra, we detected an Fe(II)-doublet, Fe(III)-doublet, and Fe(II)-octet (Figure 2). The Fe(II)-doublet at 6 K is representative of Fe(II) in phyllosilicates and/or Fe(II) adsorbed to non-Fe minerals (Dyar et al., 2008; Murad & Cashion, 2011; Williams & Scherer, 2004). The Fe(III)-doublet represents Fe(III) in phyllosilicates or bound to organic matter (Murad & Cashion, 2011; Schwertmann et al., 2005). The Fe(II)-octet is representative of Fe(II) in Fe-rich phyllosilicates (Rancourt et al., 1994; Ribeiro et al., 2009; Rothwell et al., 2023) and was included since XRD patterns (Figure S10 in Supporting Information S1) and Fe *K*-edge EXAFS data (Figure S3 in Supporting Information S1) of the initial soil showed high abundances of Fe in phyllosilicates. An additional Fe(III) sextet component was observed exclusively in the samples with addition of ^{57}Fe-enriched coprecipitates (Figures 2a and 2e). The Fe(III) sextet had parameters characteristic for poorly crystalline Fe(III) (oxyhydr)oxides (Table S4 in Supporting Information S1), such as ferrihydrite (Byrne & Kappler, 2022; Cornell & Schwertmann, 2003). The relative area of the Fe(III) sextet in the sample at t_0 was 44%, close to the calculated initial contribution of ^{57}Fe-enriched coprecipitates to the overall signal (51%, see Text S10 in Supporting Information S1). Furthermore, the spectra of initial coprecipitates also show formation of a sextet component at lower temperatures (Figure S2 in Supporting Information S1). This suggests that the entire Fe(III) sextet component is indicative of the contribution of coprecipitates to the solid ^{57}Fe pool. After 42 days of incubation, the area of the Fe(III) sextet decreased to 34% (Figures 2b and 2e). The difference in relative abundance compared with t_0 thus indicates that the added Fe(III)-OC coprecipitates were partially reduced by 22%. Based on the aqueous and solid phase analyses, we therefore found that added Fe(III)-OC coprecipitates were available for microbial reduction and the associated OC did not hinder microbial access to Fe(III).

21698961, 2025, 3, Downloaded from https://agupubs.onlinelibrary.wiley.com/doi/10.1029/2024JG008650 by Université de Neuchâtel, Wiley Online Library on [03/02/2026]. See the Terms and Conditions (https://onlinelibrary.wiley.com/terms-and-conditions) on Wiley Online Library for rules of use; OA articles are governed by the applicable Creative Commons License

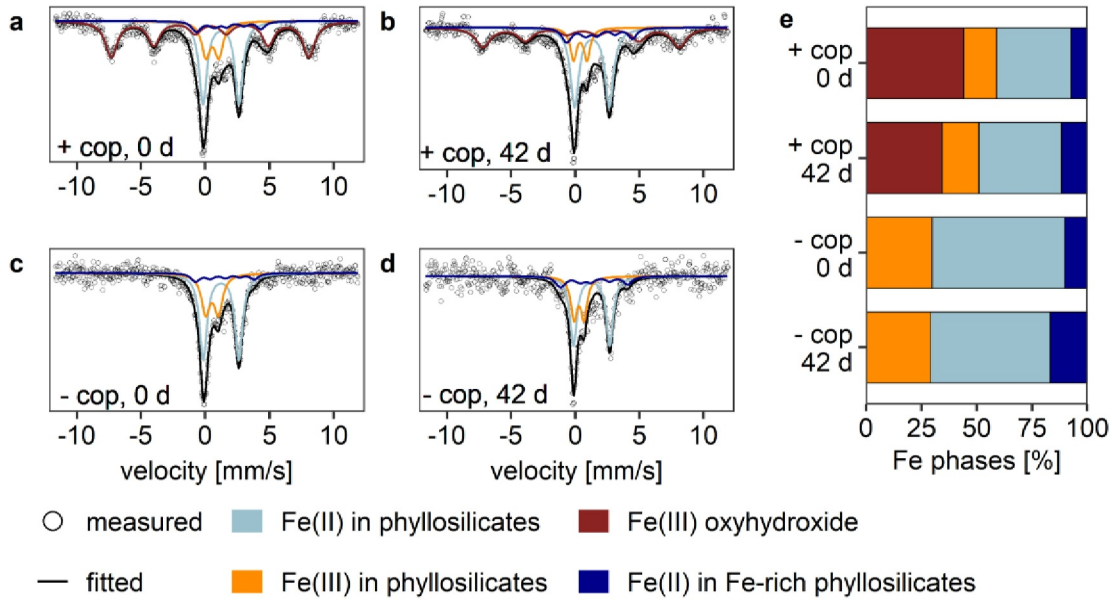

Figure 2. Solid-phase Fe speciation in soil from microcosm experiment measured by ^{57}Fe Mössbauer spectroscopy at 6 K. Subplots display spectra of soil with addition of ^{57}Fe-enriched Fe(III)-OC coprecipitates at t_0 (a) and after 42 days (b) as well as a no-coprecipitate control at t_0 (c) and after 42 days (d). All spectra show the measured data (open circles), the fit (black line) and individual components (colored lines). The following components were assigned: Fe(II) in phyllosilicates and/or adsorbed Fe (II) (light blue), Fe(III) in phyllosilicates (orange), poorly crystalline Fe(III) oxyhydroxides (dark red), Fe(II) in Fe-rich phyllosilicates (dark blue). Fitting parameters are given in Table S4 in Supporting Information S1. The relative share of each component based on area (e).

3.2. Reduction of Fe(III)-OC Coprecipitates Suppresses CH_4 Release and Increases CO_2 Emissions in Microcosm Experiments

Greenhouse gas fluxes of CH_4 and CO_2 were measured throughout the microcosm experiment. During the incubation period before coprecipitate addition (35 days) both soils had similar gas fluxes (Figure S11 in Supporting Information S1). After addition of ^{57}Fe -enriched coprecipitates, no CH_4 emissions were initially detected in the both treatments. After 8 days, CH_4 fluxes started to increase in the no-coprecipitate treatment from 0.03 ± 0.01 to 0.27 ± 0.04 µmol d^{-1} g^{-1} dry weight after 42 days (Figure S11 in Supporting Information S1). Resulting cumulative fluxes reached 4.61 ± 0.62 µmol g^{-1} dry weight after 42 days (Figure 3a). In contrast, CH_4 fluxes in the treatment with added coprecipitates stayed significantly lower between 8 and 42 days ($F = 52$, df = 7, $p < 0.05$)

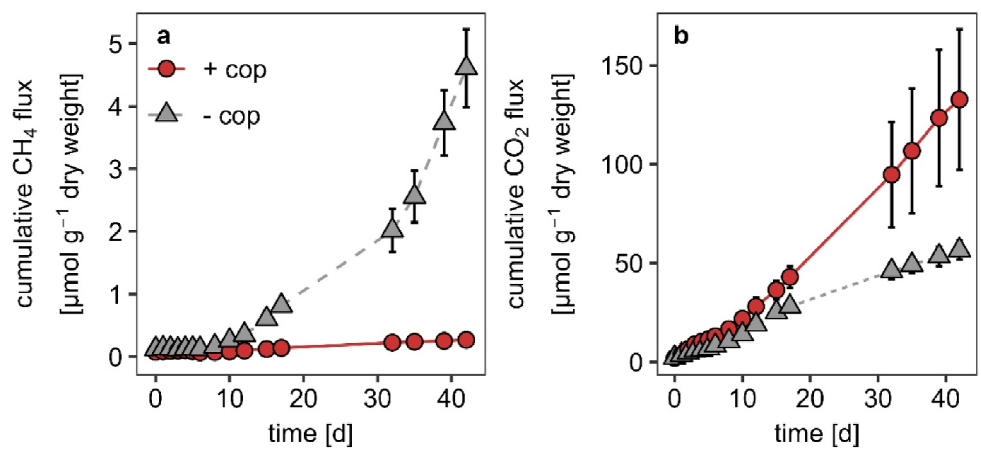

Figure 3. Cumulative greenhouse gas emissions of CH_4 (a) and CO_2 (b) in microcosm experiments with addition of ^{57}Fe-enriched Fe(III)-OC coprecipitates ("+ cop") and without ("− cop") over time. All data symbols and error bars represent the average and standard deviation of experimental triplicates, respectively.

21698961, 2025, 3, Downloaded from https://agupubs.onlinelibrary.wiley.com/doi/10.1029/2024JG008650 by Université de Neuchâtel, Wiley Online Library on [03/02/2026]. See the Terms and Conditions (https://onlinelibrary.wiley.com/terms-and-conditions) on Wiley Online Library for rules of use; OA articles are governed by the applicable Creative Commons License

21698961, 2025, 3, Downloaded from https://agupubs.onlinelibrary.wiley.com/doi/10.1029/2024JG008650 by Université de Neuchâtel, Wiley Online Library on [03/02/2026]. See the Terms and Conditions (https://onlinelibrary.wiley.com/terms-and-conditions) on Wiley Online Library for rules of use; OA articles are governed by the applicable Creative Commons License

and reached a cumulative flux of 0.27 ± 0.03 μmol g^{-1} dry weight after 42 days. This constitutes a suppression of methane emissions by 94% compared to the no-coprecipitate treatment (Figure 3a).

Microbial Fe(III) reduction likely inhibited methanogenesis, as shown in other studies based on field measurements and addition of Fe minerals to peatland soils (Lipson et al., 2012; Miller et al., 2015; Reiche et al., 2008). Previously reported methane emission rates were decreased by 37%–54% due to Fe(III) addition in the form of dissolved Fe(III)-NTA (Miller et al., 2015) and poorly crystalline ferrihydrite (Reiche et al., 2008). Our detected suppression effect might be considerably higher due to lower DOC concentrations in the coprecipitate-added treatment compared to the no-coprecipitate treatment (Figure S4g in Supporting Information S1) which can intensify the suppression effect (Sulman et al., 2022). The addition of coprecipitates likely led to initial adsorption of native DOC, as observed in other anaerobic incubations after the addition of Fe(III)-(oxyhydr)oxides (ThomasArrigo et al., 2023). The stronger decrease in CH_4 emission might also be due to anaerobic oxidation of CH_4 coupled to either Fe(III) reduction or to OC reduction which was present within the coprecipitates. Overall, our results show for the first time that Fe(III)-OC associations suppress CH_4 release in thawed permafrost peatlands, unaffected by the presence of Fe-bound OC.

Cumulative CO_2 emissions continuously increased in both treatments (Figure 3b). There was a significantly higher cumulative flux after 42 days in the treatment with added coprecipitates than in the no-coprecipitate control (132.7 ± 35.5 compared with 56.6 ± 4.7 μmol g^{-1} dry weight, $F = 14$, df = 1, $p < 0.05$). The addition of Fe(III)-OC coprecipitates thus increased cumulative CO_2 emission by 134%. Assuming that 4 mol of Fe(III) are reduced per 1 mol CO_2 produced (Küsel et al., 2008; Lipson et al., 2013; Roden & Wetzel, 1996), we calculated the contribution of Fe(III) reduction to overall anaerobic respiration using our data from the microcosm experiment (Text S11 in Supporting Information S1). Direct oxidation of OC to CO_2 via Fe(III) reduction of the coprecipitates could account, on average, for 37% of the additionally produced cumulative CO_2 flux after 42 days in the coprecipitate-added treatment compared to the no-coprecipitate control. Release of Fe-bound OC to the aqueous phase during reduction could have contributed to the remaining share of additional CO_2 emissions. Overall, the contribution of Fe-bound OC to the total soil OC pool was low (5%) but could have impacted the DOC pool. We did detect a slight increase in DOC in the coprecipitate-added treatment compared with the control (18.6 ± 1.1 compared with 14.1 ± 0.8 mg C L^{-1} after 42 days, Figure S4g in Supporting Information S1) which likely stems from Fe-bound OC. The additional DOC could have served as an electron donor for many other microorganisms, thus leading to more CO_2 emissions than expected based on Fe(III) reduction alone.

3.3. Inhibition of Methanogens and Partial Stimulation of Methanotrophs Are Responsible for Decrease in Net CH_4 Release in Microcosm Experiment

We analyzed the change in overall microbial community using 16S rRNA (gene) amplicon sequencing and compared relative abundances of known methanogens and methanotrophs. Detected methanogens generally had a significantly lower relative abundance in coprecipitate-added treatments than in the no-coprecipitate control ($F = 13$, df = 1, $p < 0.01$), with the highest difference in RNA-based abundances after 42 days (1.57 ± 0.13% compared with 2.69 ± 0.19%, $F = 17$, df = 5, $p < 0.001$, Figure 4a). Relative abundances of genera *Methanosaeta* and *Methanoregula* decreased on average by 45% and 51%, respectively, compared with the no-coprecipitate control. *Methanosarcina* had significantly lower RNA-based relative abundances in coprecipitate-added treatments after 42 days compared with control treatments (0.08 ± 0.00% to 0.30 ± 0.16%, $F = 3$, df = 5, $p < 0.05$). Concurrently, we also found differences in gene copy numbers of *mcrA* between the coprecipitate-added treatment and the no-coprecipitate control using a qPCR-based analysis (Figure 4b). DNA- and RNA-based copy numbers of the *mcrA* gene decreased over time in the treatment with added coprecipitates relative to the no-coprecipitate control. The decrease relative to the control was highest after 42 days for both DNA- and RNA-based abundances (log_2FC: −0.50 ± 0.21 and −2.54 ± 0.64, respectively, Figure 4b).

Both molecular biology techniques therefore provide novel direct evidence that the activity and abundance of methanogens was suppressed by microbial Fe(III) reduction of Fe(III)-OC coprecipitates in thawed permafrost soils. Known acetoclastic methanogens, such as genera *Methanosaeta* and *Methanosarcina* (Kurth et al., 2020), were likely more affected compared with other hydrogenotrophic or possibly methylotrophic prokaryotes (*Methanobacterium* spp.) due to substrate competiton with Fe(III)-reducing microorganisms using acetate. This is supported by the following factors: (a) constant concentrations of methanol, which did not vary between treatments (Figure S12 in Supporting Information S1), and (b) the presence of Fe(III)-reducing taxa capable of

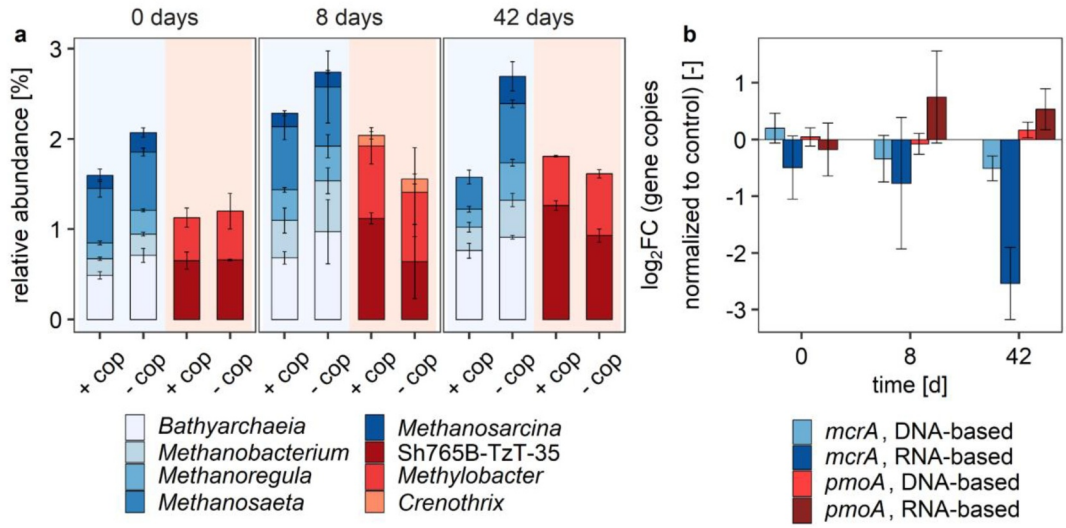

Figure 4. Changes in potential activity of methanogens and methanotrophs based on 16S rRNA sequencing and functional gene abundance in the microcosm experiment after 0, 8, and 42 days after addition of Fe(III)-OC coprecipitates. Relative 16S rRNA abundances of likely active (RNA-based) microbial taxa related to methane production (blue) and methane oxidation (red) per timepoint and treatment (+cop: with addition of Fe(III)-OC coprecipitates, -cop: no-coprecipitate control) (a). Taxa with an abundance lower than 0.1% were not included. Taxa are labeled at the genus-level, except for *Bathyarchaeia* for which no genus could be classified. DNA-based 16S rRNA abundances show similar trends and are given in Figure S13 in Supporting Information S1. Data bars and error bars represent the average and standard deviation of experimental triplicates, respectively. Quantitative PCR results of DNA- and RNA-based *mcrA* and *pmoA* gene copies (b). Changes in the coprecipitate-added treatment are displayed as the $\log_2$ fold change (FC) of the mean copy numbers of "+ cop" treatment to the mean of the no-coprecipitate control [copies$_{+cop}$ g^{-1} dry soil/copies$_{-cop}$ g^{-1} dry soil] at the same time point. Absolute gene copy numbers are displayed in Figure S14 in Supporting Information S1. Data bars and error bars represent the average and 95% confidence interval of experimental triplicates, respectively.

utilizing acetate (*Geobacter*, *Rhodoferax*, *Geothrix*, see Figure S7 in Supporting Information S1) (Coates et al., 1996, 1999; Finneran, 2003). We note that absolute acetate concentrations did not differ between treatments over time (Figure S12 in Supporting Information S1); we speculate that this is due to the utilization of acetate for Fe(III) reduction instead of methanogenesis.

We also detected both canonically aerobic methanotrophs and (putatively) anaerobic methanotrophs. Prominent aerobic methanotrophs (>0.1%) belonged to the genera of *Methylobacter* and *Crenothrix* of the order *Methylococcales* (Figure 4a). The most prominent anaerobic methanotroph was a member of the order *Methylomirabilales* (genus: Sh765B-TzT-35). Members of the *Methylomirabilales* taxa had a higher relative abundance in the coprecipitate added treatment compared with the control after 8 days (1.12 ± 0.06% compared with 0.64 ± 0.41%) and 42 days (1.26 ± 0.05% compared with 0.93 ± 0.07%). Although these differences were not statistically significant (Kruskal-Wallis test, $p = 0.15$), it is interesting to note that the RNA-based copy numbers of the *pmoA* gene were also slightly elevated at the same time points compared with the no-coprecipitate control ($\log_2$FC: 0.75 ± 0.81 and 0.54 ± 0.36 after 8 and 42 days, respectively, Figure 4b). The available genomes of *Methylomirabilales* contain genes encoding for particulate methane monooxygenase (Versantvoort et al., 2018), meaning that they could have contributed to the higher *pmoA* gene copy numbers. One member of the *Methylomirabilales* taxa, Candidatus *Methylomirabilis oxyfera*, is capable of producing dioxygen (O_2) intercellularly from nitrite to oxidize CH_4 under anoxic conditons (Ettwig et al., 2010). Additionally, it has been shown that Fe (III) oxyhydroxides can serve as an electron acceptor for methanotrophs capable of extracellular electron transfer (Rissanen et al., 2021). We therefore speculate that anaerobic methane oxidation coupled to Fe(III) or OC reduction stemming from the coprecipitates could have further inhibited net methane release and would therefore provide a previously unexplored biogeochemical pathway in terrestrial permafrost soils. The overall data, however, suggests that methanogenesis inhibition due to substrate competition with Fe(III)-reducers was the dominant process in decreasing methane emissions.

21698961, 2025, 3, Downloaded from https://agupubs.onlinelibrary.wiley.com/doi/10.1029/2024JG008650 by Université de Neuchâtel, Wiley Online Library on [03/02/2026]. See the Terms and Conditions (https://onlinelibrary.wiley.com/terms-and-conditions) on Wiley Online Library for rules of use; OA articles are governed by the applicable Creative Commons License

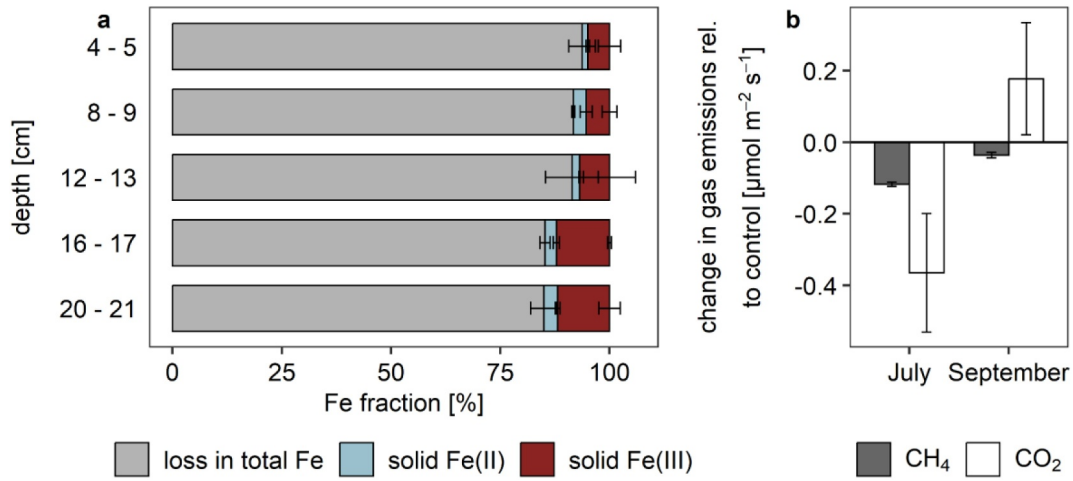

Figure 5. In situ loss and speciation of ^{NA}Fe(III)-OC coprecipitates and the net impact on greenhouse gas emissions over a growing season in the fen area of Stordalen Mire. The Fe speciation in the solid (measured) and the loss of total Fe compared with initial addition (calculated) is displayed over depth from the soil surface (a). Changes in CH_4 and CO_2 emissions [µmol m^{-2} s^{-1}] within one day after addition of ^{NA}Fe(III)-OC coprecipitates (July) and after 53 days (September) are shown relative to a no-coprecipitate plot in which only deionized water was added (b). Absolute Fe concentrations and gas flux data are provided in Figures S15 and S17 in Supporting Information S1, respectively. Data bars and error bars represent the average and range of experimental duplicates in case of the Fe speciation data, and the average and standard deviation of triplicate measurements of one "+ cop" plot and one control plot in case of the gas data.

3.4. Fe(III)-OC Coprecipitates Decrease Net CH_4 Emissions Under In Situ Conditions

To test whether our results from the microcosm experiment also apply in the environment, we incubated ^{NA}Fe(III)-OC coprecipitates in passive porewater samplers ("peepers") over a growing season in the fen area of Stordalen Mire. After the incubation time of 53 days (from July to September 2022), the solid phase data showed that the majority of added Fe in the coprecipitate-added plots was not recovered from the peepers. Suspension concentrations of total Fe were 29.6 ± 12.7 mg L^{-1} per cell across all depths (Figure S15 in Supporting Information S1) compared with the initial addition of 280 mg Fe L^{-1}. Over depth, solid total Fe concentrations increased from 17.6 ± 8.4 mg L^{-1} at 4 cm depth to 42.1 ± 8.34 mg L^{-1} at 20 cm depth (Figure S15 in Supporting Information S1). The Fe oxidation state of the remaining ^{NA}Fe(III)-OC coprecipitates was 14%–49% Fe(II) (Figure 5a). Assuming that the loss in total Fe and solid-phase Fe(II) content represents the combined extent of reductive dissolution of ^{NA}Fe(III)-OC coprecipitates, 92 ± 4.0% of Fe in coprecipitates was reduced across all depths (Figure 5a).

We also considered that some Fe(III)-OC coprecipitates might have passed the 8 µm membrane due to potentially lower aggregate size. However, in a control experiment we found that 98.9% of the initial ^{NA}Fe(III)-OC coprecipitate suspension was retained on the membrane, suggesting that the majority of the loss in Fe(III)-OC was due to reductive dissolution. The control peeper, in which no Fe(III) was added, contained lower concentrations of solid, primarily ferrous, Fe (0.65–6.31 mg L^{-1}, Figure S15 in Supporting Information S1) across all depths. This suggests that there was a low background concentration of particulate Fe in the porewater. We did not detect any large differences in dissolved species concentrations between the two treatments at the end of the experiment. Aqueous Fe^{2+}, dissolved CH_4, and DOC did not vary in comparison to the no-coprecipitate treatment (Figure S16 in Supporting Information S1). It is likely that any initial changes in porewater chemistry inside the peeper cells due to Fe(III) reduction were overridden by re-equilibration with the soil porewater.

The reduction extent of our added Fe(III)-OC coprecipitates under in situ conditions was thus substantially larger than in the microcosm experiment. The following factors might have played a role: (a) The in situ DOC concentrations detected in all three peepers were, on average, at least three times higher in the field compared to the microcosm experiment (31.9 ± 8.6 mg C L^{-1} compared with 8.8 ± 5.7 mg C L^{-1}, respectively). The higher DOC concentrations might have facilitated more Fe(III) reduction via OC oxidation relative to the microcosm experiment. (b) The peepers reached from 4 to 21 cm from the soil surface, while the soil used for the microcosm experiment came from a depth of 30 cm. Thus, the geochemical parameters (such as OC content, pH, presence of

21698961, 2025, 3, Downloaded from https://agupubs.onlinelibrary.wiley.com/doi/10.1029/2024JG008650 by Université de Neuchâtel, Wiley Online Library on [03/02/2026]. See the Terms and Conditions (https://onlinelibrary.wiley.com/terms-and-conditions) on Wiley Online Library for rules of use; OA articles are governed by the applicable Creative Commons License

21698961, 2025, 3, Downloaded from https://agupubs.onlinelibrary.wiley.com/doi/10.1029/2024JG008650 by Université de Neuchâtel, Wiley Online Library on [03/02/2026]. See the Terms and Conditions (https://onlinelibrary.wiley.com/terms-and-conditions) on Wiley Online Library for rules of use; OA articles are governed by the applicable Creative Commons License

other nutrients like phosphate and nitrate) and the microbial community might have slightly differed. (c) Under waterlogged conditions in the soil, we expect that there was constant, albeit slow, exchange of nutrients over the time span of the experiment, such that conditions for microbial Fe(III) reduction might be more favorable. (d) It is also possible that we recovered less of the added coprecipitates than expected. Microbial reduction of coprecipiates could have decreased their particle size such that they could pass the membrane of the peeper.

Our quantified extent of Fe(III) reduction of Fe(III)-OC coprecipitates is substantially higher than that of a previous experiment at the same site by Patzner, Kainz, et al. (2022). They estimated that 50 ± 12% of added Fe (III) in form of ferrihydrite coated on sand grains was reduced over a summer season (from June to September) in the fen area. The reduction extent of our added ^{NA}Fe(III)-OC coprecipitates might have been higher due to the more poorly crystalline mineral structure of coprecipitates compared to ferrihydrite, making them more reactive (Eusterhues et al., 2008; Schwertmann et al., 2005), and the fact that coating of ferrihydrite on sand grains might make the mineral less susceptible to microbial reduction (Masue-Slowey et al., 2011). The presence of associated OC within the Fe mineral therefore increased the reduction extent with possible feedbacks on net CH_4 release.

The GHG fluxes measured above the different peeper treatments changed significantly depending on the season ($F = 18$, df $= 1$, $p < 0.05$), with lower CH_4 and CO_2 emissions in September than in July (Figure S17 in Supporting Information S1). We thus examined the differences in net fluxes of the coprecipitate-added and no-coprecipitate plot at each sampling time. Net CH_4 emission in the coprecipitated plot relative to the no-coprecipitate plot decreased significantly by 40% within one day after addition of coprecipitates (change of -0.12 ± 0.01 μmol m^{-2} s^{-1}) and by 33% at the end of the growing season (-0.04 ± 0.01 μmol m^{-2} s^{-1}, Figure 5b). Methanogenesis was thus inhibited likely due to Fe(III) reduction of added ^{NA}Fe(III)-OC coprecipitates, matching with the results of our microcosm experiment. Since spatial heterogeneity of CH_4 fluxes in peatlands is high (Taylor et al., 2023), we cannot rule out that initial differences in CH_4 fluxes between the coprecipitate-added and control plot contributed to the measured differences in CH_4 emissions. However, we took care to choose plots with similar vegetation composition (Figure S6 in Supporting Information S1) and only 1 m apart in order to minimize differences in soil temperatures.

Fluxes of CO_2 measured under dark conditions (excluding photosynthesis) initially slightly decreased as a consequence of ^{NA}Fe(III)-OC coprecipitate addition by 25% (-0.37 ± 0.17 μmol m^{-2} s^{-1}, Figure 5b) relative to the no-coprecipitate plot. In September, fluxes were on average 36% higher relative to the no-coprecipitate control (0.18 ± 0.15 μmol m^{-2} s^{-1}). It is likely the ^{NA}Fe(III)-OC coprecipitates initially bound additional DOC, as detected in the microcosm experiment (Figure S4 in Supporting Information S1). This could have decreased CO_2 fluxes, which are often controlled by DOC concentrations (Algesten et al., 2005). As ^{NA}Fe(III)-OC coprecipitates were reductively dissolved, they likely released this adsorbed OC again, contributing to an increased CO_2 flux together with microbial Fe(III) reduction coupled to OC oxidation. Our data thus show that Fe(III)-OC coprecipitates also decrease net methane release in situ, which constitutes the first time this process is shown in thawed permafrost soils.

4. Conclusions

This study demonstrated that the addition of Fe(III)-OC associations (in the form of coprecipitates) in anoxic permafrost peatland soils decreases net CH_4 emissions (Figure 6). In both our microcosm and field experiment with fully thawed permafrost peatland soil, addition of synthesized Fe(III)-OC coprecipitates lowered fluxes of CH_4 compared with control treatments without the coprecipitates. Decrease in CH_4 fluxes was mainly due to inhibition of methanogenesis, likely of acetoclastic methanogens (e.g., *Methanosaeta* and *Methanosarcina*) by substrate competition with Fe(III)-reducers which reduced added Fe(III)-OC coprecipitates. Methanotrophy coupled to Fe(III) or OC reduction might have played a minor role, as suggested by the increase in relative abundance of *Methylomirabilales* spp. upon Fe(III)-OC coprecipitate addition.

The results of our study can be used to gain insights into future coupled Fe-CH_4 cycling in thawing permafrost peatlands. The areal cover of fens at Stordalen Mire has already doubled in the last 50 years (Varner et al., 2022) with this trend projected to continue in the future. Similarly, many other permafrost soils in Scandinavia and Canada, including Yedoma deposits, are prone to the formation of thermokarst lakes and wetlands (Borge et al., 2017; In 'T Zandt et al., 2020; Payette et al., 2004). A large proportion of these previously oxic soils could abruptly thaw and collapse in the future (Turetsky et al., 2020), establishing anoxic conditions. It is expected that a majority of the radiative forcing under these conditions will stem from CH_4 (Knoblauch et al., 2018; Turetsky

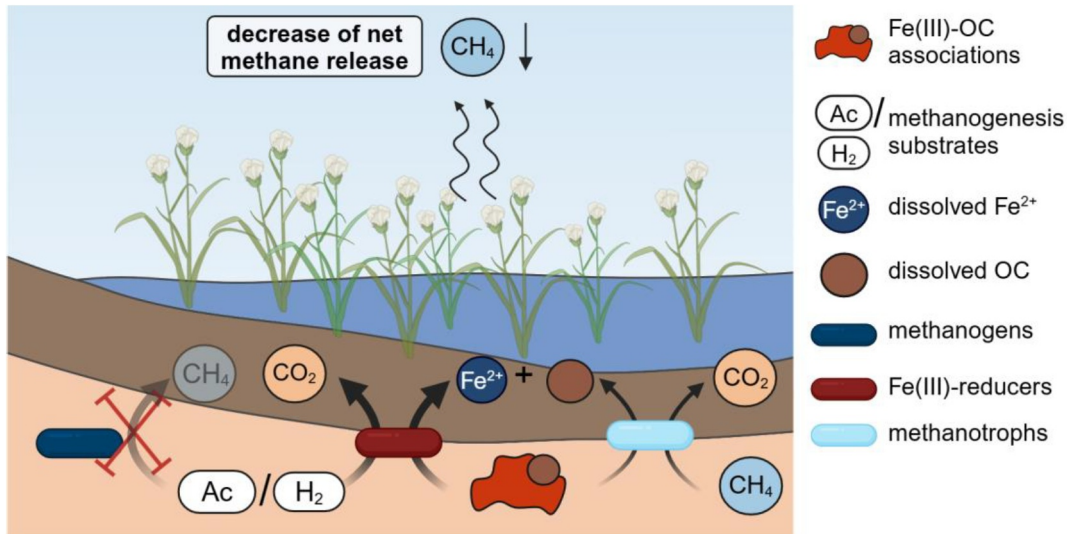

Figure 6. Schematic representation of processes influencing net methane release in thawed permafrost soils due to Fe(III)-organic carbon (OC) associations. Net methane release from soils is decreased by reduction of Fe(III)-OC associations due to two processes: (1) reduction of Fe(III)-OC associations by Fe(III)-reducing microorganisms thermodynamically inhibits methanogens and scavenges substrates for methanogenesis, and (2) methanotrophic microorganisms likely use Fe(III) or released dissolved OC as an electron acceptor to perform anaerobic methane oxidation.

Acknowledgments
This work was funded by the German Research foundation (DFG, KA 1736/66-1). A.K. acknowledges infrastructural support by the DFG under Germany's Excellence Strategy, cluster of Excellence EXC2124, project ID 390838134. We would like to thank the Swedish Polar Research Secretariat and SITES for the support of the work done at the Abisko Scientific Research Station. Special thanks go to Emily Pederson for her excellent help in the organization of the field campaign. We are also grateful to Sören Drabesch for discussions on gas analysis and Marie Mollenkopf for her assistance during field work and helpful data discussions. We thank Hayley Green for laboratory assistance and Maike Friedel, Katrin Wunsch, and Ankita Chauhan for assistance during the field work. We are grateful to Alex Schnapper and Marc Jantz for construction of the passive porewater samplers. We thank Mette Svenning for the use of her gas chambers during the field campaigns. We acknowledge SOLEIL (proposal nr. 20221355) for the use of the synchrotron radiation facilities and thank Gautier Landrot (SAMBA beamline) for his help during the synchrotron data collection. We thank Thomas Borch for providing the XAS spectra of Fe-OC references. Furthermore, we are grateful for the help provided by Tsz Ho Chiu for freeze-drying and XRD measurement, Franziska Schädler for molecular biology analyses, and Heinrich Taubald for XRF measurements. Sequencing was supported by the Institute for Medical Microbiology and Hygiene (MGM) of the University of Tübingen. Open Access funding enabled and organized by Projekt DEAL.

et al., 2020). Our findings show that native Fe(III)-OC associations could attenuate CH_4 release for a certain time frame, and thus decrease the radiative forcing by emitting more C as CO_2. The timescale of this attenuation is still highly uncertain due to limited data on Fe stocks in permafrost peatlands (Mu et al., 2016; Patzner et al., 2020) and the estimated in situ Fe reduction rates (Lipson et al., 2013). In addition, Fe(II)-oxidizing microorganisms could play a role in replenishing the content of Fe(III)-OC associations in permanently anoxic soils, as they have been detected in other Arctic habitats (Emerson et al., 2015).

The results of our two experiments also showcase the sensitivity of CH_4 release on substrate availability and microbial composition of methane-cycling and Fe-cycling communities. If higher substrate concentrations are available and/or methanogenic communitites are made up of metabolically flexible members, competition with Fe(III)-reducing microorganisms might be decreased and methanogenesis suppression might be less severe. Our work also has implications for other flooded soils in which high OC contents, Fe minerals, and methanogenesis are expected, such as paddy soils or coastal marshes. Since these soils experience periodic flooding, abiotic or microbial re-oxidation of Fe(II) might regenerate Fe(III)-OC associations that may suppress CH_4 emission long term. Thus, Fe(III)-OC associations may play a major role in CH_4 emissions from a range of flooded (or redox-dynamic) soils.

Data Availability Statement

All data displayed in the figures are available at Zenodo (https://doi.org/10.5281/zenodo.14826148) and raw sequencing data have been deposited at NCBI in the Sequence Read Archive (SRA) under BioProject accession number PRJNA1123917 (https://www.ncbi.nlm.nih.gov/bioproject/PRJNA1123917). The samples discussed here are SAMN41832410 - SAMN41832445 (sample title contains “fen”).

References

Achtnich, C., Bak, F., & Conrad, R. (1995). Competition for electron donors among nitrate reducers, ferric iron reducers, sulfate reducers, and methanogens in anoxic paddy soil. *Biology and Fertility of Soils*, *19*(1), 65–72. https://doi.org/10.1007/BF00336349

Adhikari, D., Zhao, Q., Das, K., Mejia, J., Huang, R., Wang, X., et al. (2017). Dynamics of ferrihydrite-bound organic carbon during microbial Fe reduction. *Geochimica et Cosmochimica Acta*, *212*, 221–233. https://doi.org/10.1016/j.gca.2017.06.017

Algesten, G., Sobek, S., Bergström, A.-K., Jonsson, A., Tranvik, L. J., & Jansson, M. (2005). Contribution of sediment respiration to summer CO2 emission from low productive boreal and subarctic lakes. *Microbial Ecology*, *50*(4), 529–535. https://doi.org/10.1007/s00248-005-5007-x

Apprill, A., McNally, S., Parsons, R., & Weber, L. (2015). Minor revision to V4 region SSU rRNA 806R gene primer greatly increases detection of SAR11 bacterioplankton. *Aquatic Microbial Ecology*, *75*(2), 129–137. https://doi.org/10.3354/ame01753

21698961, 2025, 3, Downloaded from https://agupubs.onlinelibrary.wiley.com/doi/10.1029/2024JG008650 by Université de Neuchâtel, Wiley Online Library on [03/02/2026]. See the Terms and Conditions (https://onlinelibrary.wiley.com/terms-and-conditions) on Wiley Online Library for rules of use; OA articles are governed by the applicable Creative Commons License

Bar-Or, I., Elvert, M., Eckert, W., Kushmaro, A., Vigderovich, H., Zhu, Q., et al. (2017). Iron-coupled anaerobic oxidation of methane performed by a mixed bacterial-archaeal community based on poorly reactive minerals. *Environmental Science & Technology*, *51*(21), 12293–12301. https://doi.org/10.1021/acs.est.7b03126

Borge, A. F., Westermann, S., Solheim, I., & Etzelmüller, B. (2017). Strong degradation of palsas and peat plateaus in northern Norway during the last 60 years. *The Cryosphere*, *11*(1), 1–16. https://doi.org/10.5194/tc-11-1-2017

Bowes, H. L., & Hornibrook, E. R. C. (2006). Emission of highly ^{13}C-depleted methane from an upland blanket mire. *Geophysical Research Letters*, *33*(4), 2005GL025209. https://doi.org/10.1029/2005GL025209

Bridgham, S. D., Cadillo-Quiroz, H., Keller, J. K., & Zhuang, Q. (2013). Methane emissions from wetlands: Biogeochemical, microbial, and modeling perspectives from local to global scales. *Global Change Biology*, *19*(5), 1325–1346. https://doi.org/10.1111/gcb.12131

Byrne, J. M., & Kappler, A. (2022). A revised analysis of ferrihydrite at liquid helium temperature using Mössbauer spectroscopy. *American Mineralogist*, *107*(8), 1643–1651. https://doi.org/10.2138/am-2021-7802

Coates, J. D., Ellis, D. J., Gaw, C. V., & Lovley, D. R. (1999). Geothrix fermentans gen. Nov., sp. Nov., a novel Fe(III)-reducing bacterium from a hydrocarbon-contaminated aquifer. *International Journal of Systematic and Evolutionary Microbiology*, *49*(4), 1615–1622. https://doi.org/10.1099/00207713-49-4-1615

Coates, J. D., Phillips, E. J., Lonergan, D. J., Jenter, H., & Lovley, D. R. (1996). Isolation of Geobacter species from diverse sedimentary environments. *Applied and Environmental Microbiology*, *62*(5), 1531–1536. https://doi.org/10.1128/aem.62.5.1531-1536.1996

Cooper, R. E., Eusterhues, K., Wegner, C.-E., Totsche, K. U., & Küsel, K. (2017). Ferrihydrite-associated organic matter (OM) stimulates reduction by Shewanella oneidensis MR-1 and a complex microbial consortia. *Biogeosciences*, *14*(22), 5171–5188. https://doi.org/10.5194/bg-14-5171-2017

Cornell, R. M., & Schwertmann, U. (2003). *The iron oxides (2., completely rev. and extended)*. Wiley VCH. https://doi.org/10.1002/3527602097

Dong, H., Zeng, Q., Sheng, Y., Chen, C., Yu, G., & Kappler, A. (2023). Coupled iron cycling and organic matter transformation across redox interfaces. *Nature Reviews Earth & Environment*, *4*(9), 659–673. https://doi.org/10.1038/s43017-023-00470-5

Drake, H. L., Horn, M. A., & Wüst, P. K. (2009). Intermediary ecosystem metabolism as a main driver of methanogenesis in acidic wetland soil. *Environmental Microbiology Reports*, *1*(5), 307–318. https://doi.org/10.1111/j.1758-2229.2009.00050.x

Dyar, M. D., Schaefer, M. W., Sklute, E. C., & Bishop, J. L. (2008). Mössbauer spectroscopy of phyllosilicates: Effects of fitting models on recoil-free fractions and redox ratios. *Clay Minerals*, *43*(1), 3–33. https://doi.org/10.1180/claymin.2008.043.1.02

Emerson, D., Scott, J. J., Benes, J., & Bowden, W. B. (2015). Microbial iron oxidation in the Arctic tundra and its implications for biogeochemical cycling. *Applied and Environmental Microbiology*, *81*(23), 8066–8075. https://doi.org/10.1128/AEM.02832-15

Ettwig, K. F., Butler, M. K., Le Paslier, D., Pelletier, E., Mangenot, S., Kuypers, M. M. M., et al. (2010). Nitrite-driven anaerobic methane oxidation by oxygenic bacteria. *Nature*, *464*(7288), 543–548. https://doi.org/10.1038/nature08883

Ettwig, K. F., Zhu, B., Speth, D., Keltjens, J. T., Jetten, M. S. M., & Kartal, B. (2016). Archaea catalyze iron-dependent anaerobic oxidation of methane. *Proceedings of the National Academy of Sciences*, *113*(45), 12792–12796. https://doi.org/10.1073/pnas.1609534113

Eusterhues, K., Hädrich, A., Neidhardt, J., Küsel, K., Keller, T. F., Jandt, K. D., & Totsche, K. U. (2014). Reduction of ferrihydrite with adsorbed and coprecipitated organic matter: Microbial reduction by Geobacter bremensis vs. Abiotic reduction by Na-dithionite. *Biogeosciences*, *11*(18), 4953–4966. https://doi.org/10.5194/bg-11-4953-2014

Eusterhues, K., Wagner, F. E., Häusler, W., Hanzlik, M., Knicker, H., Totsche, K. U., et al. (2008). Characterization of ferrihydrite-soil organic matter coprecipitates by X-ray diffraction and Mössbauer spectroscopy. *Environmental Science & Technology*, *42*(21), 7891–7897. https://doi.org/10.1021/es800881w

Ewels, P. A., Peltzer, A., Fillinger, S., Patel, H., Alneberg, J., Wilm, A., et al. (2020). The nf-core framework for community-curated bioinformatics pipelines. *Nature Biotechnology*, *38*(3), 276–278. https://doi.org/10.1038/s41587-020-0439-x

Farquharson, L. M., Romanovsky, V. E., Cable, W. L., Walker, D. A., Kokelj, S. V., & Nicolsky, D. (2019). Climate change drives widespread and rapid thermokarst development in very cold permafrost in the Canadian high Arctic. *Geophysical Research Letters*, *46*(12), 6681–6689. https://doi.org/10.1029/2019GL082187

Finneran, K. T. (2003). Rhodoferax ferrireducens sp. Nov., a psychrotolerant, facultatively anaerobic bacterium that oxidizes acetate with the reduction of Fe(III). *International Journal of Systematic and Evolutionary Microbiology*, *53*(3), 669–673. https://doi.org/10.1099/ijs.0.02298-0

Friedrich, M. W. (2005). Methyl-coenzyme M reductase genes: Unique functional markers for methanogenic and anaerobic methane-oxidizing Archaea. In *Methods in Enzymology* (Vol. 397, pp. 428–442). Elsevier. https://doi.org/10.1016/S0076-6879(05)97026-2

Fu, L., Zhou, T., Wang, J., You, L., Lu, Y., Yu, L., & Zhou, S. (2019). NanoFe3O4 as solid electron shuttles to accelerate acetotrophic methanogenesis by Methanosarcina barkeri. *Frontiers in Microbiology*, *10*, 388. https://doi.org/10.3389/fmicb.2019.00388

Heron, G., Crouzet, C., Bourg, A. C. M., & Christensen, T. H. (1994). Speciation of Fe(II) and Fe(III) in contaminated aquifer sediments using chemical extraction techniques. *Environmental Science & Technology*, *28*(9), 1698–1705. https://doi.org/10.1021/es00058a023

Hesslein, R. H. (1976). An in situ sampler for close interval pore water studies. *Limnology & Oceanography*, *21*(6), 912–914. https://doi.org/10.4319/lo.1976.21.6.0912

In 'T Zandt, M. H., Liebner, S., & Welte, C. U. (2020). Roles of thermokarst lakes in a warming world. *Trends in Microbiology*, *28*(9), 769–779. https://doi.org/10.1016/j.tim.2020.04.002

Juottonen, H., Galand, P. E., & Yrjälä, K. (2006). Detection of methanogenic Archaea in peat: Comparison of PCR primers targeting the mcrA gene. *Research in Microbiology*, *157*(10), 914–921. https://doi.org/10.1016/j.resmic.2006.08.006

Kim, D.-G., Vargas, R., Bond-Lamberty, B., & Turetsky, M. R. (2012). Effects of soil rewetting and thawing on soil gas fluxes: A review of current literature and suggestions for future research. *Biogeosciences*, *9*(7), 2459–2483. https://doi.org/10.5194/bg-9-2459-2012

Kleinen, T., Gromov, S., Steil, B., & Brovkin, V. (2021). Atmospheric methane underestimated in future climate projections. *Environmental Research Letters*, *16*(9), 094006. https://doi.org/10.1088/1748-9326/ac1814

Knoblauch, C., Beer, C., Liebner, S., Grigoriev, M. N., & Pfeiffer, E.-M. (2018). Methane production as key to the greenhouse gas budget of thawing permafrost. *Nature Climate Change*, *8*(4), 309–312. https://doi.org/10.1038/s41558-018-0095-z

Kokelj, S. V., & Jorgenson, M. T. (2013). Advances in thermokarst research. *Permafrost and Periglacial Processes*, *24*(2), 108–119. https://doi.org/10.1002/ppp.1779

Kostka, J. E., & Luther, G. W. (1994). Partitioning and speciation of solid phase iron in saltmarsh sediments. *Geochimica et Cosmochimica Acta*, *58*(7), 1701–1710. https://doi.org/10.1016/0016-7037(94)90531-2

Kurth, J. M., Op Den Camp, H. J. M., & Welte, C. U. (2020). Several ways one goal—Methanogenesis from unconventional substrates. *Applied Microbiology and Biotechnology*, *104*(16), 6839–6854. https://doi.org/10.1007/s00253-020-10724-7

Küsel, K., Blöthe, M., Schulz, D., Reiche, M., & Drake, H. L. (2008). Microbial reduction of iron and porewater biogeochemistry in acidic peatlands. *Biogeosciences*, *5*(6), 1537–1549. https://doi.org/10.5194/bg-5-1537-2008

21698961, 2025, 3, Downloaded from https://agupubs.onlinelibrary.wiley.com/doi/10.1029/2024JG008650 by Université de Neuchâtel, Wiley Online Library on [03/02/2026]. See the Terms and Conditions (https://onlinelibrary.wiley.com/terms-and-conditions) on Wiley Online Library for rules of use; OA articles are governed by the applicable Creative Commons License

Lei, P., Chen, M., Rong, N., Tang, W., & Zhang, H. (2024). A passive sampler for synchronously measuring inorganic and organic pollutants in sediment porewater: Configuration and field application. *Journal of Environmental Sciences*, *136*, 201–212. https://doi.org/10.1016/j.jes.2023.02.019

Liebner, S., Ganzert, L., Kiss, A., Yang, S., Wagner, D., & Svenning, M. M. (2015). Shifts in methanogenic community composition and methane fluxes along the degradation of discontinuous permafrost. *Frontiers in Microbiology*, *6*, 356. https://doi.org/10.3389/fmicb.2015.00356

Lim, A. G., Loiko, S. V., & Pokrovsky, O. S. (2022). Sizable pool of labile organic carbon in peat and mineral soils of permafrost peatlands, western Siberia. *Geoderma*, *409*, 115601. https://doi.org/10.1016/j.geoderma.2021.115601

Lipson, D. A., Raab, T. K., Goria, D., & Zlamal, J. (2013). The contribution of Fe(III) and humic acid reduction to ecosystem respiration in drained thaw lake basins of the Arctic Coastal Plain. *Global Biogeochemical Cycles*, *27*(2), 399–409. https://doi.org/10.1002/gbc.20038

Lipson, D. A., Zona, D., Raab, T. K., Bozzolo, F., Mauritz, M., & Oechel, W. C. (2012). Water-table height and microtopography control biogeochemical cycling in an Arctic coastal tundra ecosystem. *Biogeosciences*, *9*(1), 577–591. https://doi.org/10.5194/bg-9-577-2012

Liu, F., Qin, S., Fang, K., Chen, L., Peng, Y., Smith, P., & Yang, Y. (2022). Divergent changes in particulate and mineral-associated organic carbon upon permafrost thaw. *Nature Communications*, *13*(1), 5073. https://doi.org/10.1038/s41467-022-32681-7

Malmer, N., Johansson, T., Olsrud, M., & Christensen, T. R. (2005). Vegetation, climatic changes and net carbon sequestration in a North-Scandinavian subarctic mire over 30 years. *Global Change Biology*, *11*(11), 1895–1909. https://doi.org/10.1111/j.1365-2486.2005.01042.x

Masue-Slowey, Y., Loeppert, R. H., & Fendorf, S. (2011). Alteration of ferrihydrite reductive dissolution and transformation by adsorbed as and structural Al: Implications for as retention. *Geochimica et Cosmochimica Acta*, *75*(3), 870–886. https://doi.org/10.1016/j.gca.2010.11.016

McDonald, I. R., Bodrossy, L., Chen, Y., & Murrell, J. C. (2008). Molecular ecology techniques for the study of aerobic methanotrophs. *Applied and Environmental Microbiology*, *74*(5), 1305–1315. https://doi.org/10.1128/AEM.02233-07

Megonigal, J. P., Hines, M. E., & Visscher, P. T. (2003). Anaerobic metabolism: Linkages to trace gases and aerobic processes. In *Treatise on geochemistry* (pp. 317–424). Elsevier. https://doi.org/10.1016/B0-08-043751-6/08132-9

Miller, K. E., Lai, C.-T., Friedman, E. S., Angenent, L. T., & Lipson, D. A. (2015). Methane suppression by iron and humic acids in soils of the Arctic Coastal Plain. *Soil Biology and Biochemistry*, *83*, 176–183. https://doi.org/10.1016/j.soilbio.2015.01.022

Monhonval, A., Strauss, J., Thomas, M., Hirst, C., Titeux, H., Louis, J., et al. (2022). Thermokarst processes increase the supply of stabilizing surfaces and elements (Fe, Mn, Al, and Ca) for mineral–organic carbon interactions. *Permafrost and Periglacial Processes*, *33*(4), 452–469. https://doi.org/10.1002/ppp.2162

Mu, C. C., Zhang, T. J., Zhao, Q., Guo, H., Zhong, W., Su, H., & Wu, Q. B. (2016). Soil organic carbon stabilization by iron in permafrost regions of the Qinghai-Tibet Plateau. *Geophysical Research Letters*, *43*(19), 10286–10294. https://doi.org/10.1002/2016GL070071

Mueller, C. W., Rethemeyer, J., Kao-Kniffin, J., Löppmann, S., Hinkel, K. M., & G. Bockheim, J. (2015). Large amounts of labile organic carbon in permafrost soils of northern A laska. *Global Change Biology*, *21*(7), 2804–2817. https://doi.org/10.1111/gcb.12876

Murad, E., & Cashion, J. (2011). *Mössbauer spectroscopy of environmental materials and their industrial utilization*. Springer.

Otte, J. M., Blackwell, N., Soos, V., Rughöft, S., Maisch, M., Kappler, A., et al. (2018). Sterilization impacts on marine sediment—Are we able to inactivate microorganisms in environmental samples? *FEMS Microbiology Ecology*, *94*(12). https://doi.org/10.1093/femsec/fiy189

Parada, A. E., Needham, D. M., & Fuhrman, J. A. (2016). Every base matters: Assessing small subunit rRNA primers for marine microbiomes with mock communities, time series and global field samples. *Environmental Microbiology*, *18*(5), 1403–1414. https://doi.org/10.1111/1462-2920.13023

Patzner, M. S., Kainz, N., Lundin, E., Barczok, M., Smith, C., Herndon, E., et al. (2022). Seasonal fluctuations in iron cycling in thawing permafrost peatlands. *Environmental Science & Technology*, *56*(7), 4620–4631. https://doi.org/10.1021/acs.est.1c06937

Patzner, M. S., Logan, M., McKenna, A. M., Young, R. B., Zhou, Z., Joss, H., et al. (2022). Microbial iron cycling during palsa hillslope collapse promotes greenhouse gas emissions before complete permafrost thaw. *Communications Earth & Environment*, *3*(1), 76. https://doi.org/10.1038/s43247-022-00407-8

Patzner, M. S., Mueller, C. W., Malusova, M., Baur, M., Nikeleit, V., Scholten, T., et al. (2020). Iron mineral dissolution releases iron and associated organic carbon during permafrost thaw. *Nature Communications*, *11*(1), 6329. https://doi.org/10.1038/s41467-020-20102-6

Payette, S., Delwaide, A., Caccianiga, M., & Beauchemin, M. (2004). Accelerated thawing of subarctic peatland permafrost over the last 50 years. *Geophysical Research Letters*, *31*(18), 2004GL020358. https://doi.org/10.1029/2004GL020358

Rancourt, D. G., Christie, I. A. D., Lamarche, G., Swainson, I., & Flandrois, S. (1994). Magnetism of synthetic and natural annite mica: Ground state and nature of excitations in an exchange-wise two-dimensional easy-plane ferromagnet with disorder. *Journal of Magnetism and Magnetic Materials*, *138*(1–2), 31–44. https://doi.org/10.1016/0304-8853(94)90396-4

Reiche, M., Torburg, G., & Küsel, K. (2008). Competition of Fe(III) reduction and methanogenesis in an acidic fen. *FEMS Microbiology Ecology*, *65*(1), 88–101. https://doi.org/10.1111/j.1574-6941.2008.00523.x

Ribeiro, F. R., Fabris, J. D., Kostka, J. E., Komadel, P., & Stucki, J. W. (2009). Comparisons of structural iron reduction in smectites by bacteria and dithionite: II. A variable-temperature Mössbauer spectroscopic study of garfield nontronite. *Pure and Applied Chemistry*, *81*(8), 1499–1509. https://doi.org/10.1351/PAC-CON-08-11-16

Rissanen, A. J., Saarela, T., Jäntti, H., Buck, M., Peura, S., Aalto, S. L., et al. (2021). Vertical stratification patterns of methanotrophs and their genetic controllers in water columns of oxygen-stratified boreal lakes. *FEMS Microbiology Ecology*, *97*(2), fiaa252. https://doi.org/10.1093/femsec/fiaa252

Roden, E. E., & Wetzel, R. G. (1996). Organic carbon oxidation and suppression of methane production by microbial Fe(III) oxide reduction in vegetated and unvegetated freshwater wetland sediments. *Limnology & Oceanography*, *41*(8), 1733–1748. https://doi.org/10.4319/lo.1996.41.8.1733

Roden, E. E., & Wetzel, R. G. (2003). Competition between Fe(III)-Reducing and methanogenic bacteria for acetate in iron-rich freshwater sediments. *Microbial Ecology*, *45*(3), 252–258. https://doi.org/10.1007/s00248-002-1037-9

Rothwell, K. A., Pentrak, M. P., Pentrak, L. A., Stucki, J. W., & Neumann, A. (2023). Reduction pathway-dependent formation of reactive Fe(II) sites in clay minerals. *Environmental Science & Technology*, *57*(28), 10231–10241. https://doi.org/10.1021/acs.est.3c01655

Rößger, N., Sachs, T., Wille, C., Boike, J., & Kutzbach, L. (2022). Seasonal increase of methane emissions linked to warming in Siberian tundra. *Nature Climate Change*, *12*(11), 1031–1036. https://doi.org/10.1038/s41558-022-01512-4

Saunois, M., Stavert, A. R., Poulter, B., Bousquet, P., Canadell, J. G., Jackson, R. B., et al. (2020). The global methane budget 2000–2017. *Earth System Science Data*, *12*(3), 1561–1623. https://doi.org/10.5194/essd-12-1561-2020

Schwertmann, U., Wagner, F., & Knicker, H. (2005). Ferrihydrite–Humic associations. *Soil Science Society of America Journal*, *69*(4), 1009–1015. https://doi.org/10.2136/sssaj2004.0274

Stams, A. J. M., Elferink, S. J. W. H. O., & Westermann, P. (2003). *Metabolic interactions between methanogenic consortia and anaerobic respiring bacteria*. In B. K. Ahring, I. Angelidaki, E. C. De Macario, H. N. Gavala, J. Hofman-Bang, A. J. L. Macario, et al. (Vol. 81, pp. 31–56). Springer Berlin Heidelberg. https://doi.org/10.1007/3-540-45839-5_2

21698961, 2025, 3, Downloaded from https://agupubs.onlinelibrary.wiley.com/doi/10.1029/2024JG008650 by Université de Neuchâtel, Wiley Online Library on [03/02/2026]. See the Terms and Conditions (https://onlinelibrary.wiley.com/terms-and-conditions) on Wiley Online Library for rules of use; OA articles are governed by the applicable Creative Commons License

Stookey, L. L. (1970). Ferrozine—A new spectrophotometric reagent for iron. *Analytical Chemistry*, *42*(7), 779–781. https://doi.org/10.1021/ac60289a016

Straub, D., Blackwell, N., Langarica-Fuentes, A., Peltzer, A., Nahnsen, S., & Kleindienst, S. (2020). Interpretations of environmental microbial community studies are biased by the selected 16S rRNA (gene) amplicon sequencing pipeline. *Frontiers in Microbiology*, *11*, 550420. https://doi.org/10.3389/fmicb.2020.550420

Straub, D., Tångrot, J., Peltzer, A., Lundin, D., Bennett, A., Sundh, J., et al. (2024). nf-core/ampliseq: Ampliseq version 2.8.0 (version 2.8.0) [Software]. *[Object]*. https://doi.org/10.5281/ZENODO.1493841

Sulman, B. N., Yuan, F., O'Meara, T., Gu, B., Herndon, E. M., Zheng, J., et al. (2022). Simulated hydrological dynamics and coupled iron redox cycling impact methane production in an Arctic soil. *Journal of Geophysical Research: Biogeosciences*, *127*(10), e2021JG006662. https://doi.org/10.1029/2021JG006662

Sun, F.-S., Ma, C., Yu, G.-H., Kuzyakov, Y., Lang, Y.-C., Fu, P.-Q., et al. (2023). Organic carbon preservation in wetlands: Iron oxide protection vs. thermodynamic limitation. *Water Research*, *241*, 120133. https://doi.org/10.1016/j.watres.2023.120133

Taylor, M. A., Bradford, M. A., Arnold, W., Takahashi, D., Colgan, T., Davis, V., et al. (2023). Quantifying the effects sizes of common controls on methane emissions from an ombrotrophic peat bog. *Journal of Geophysical Research: Biogeosciences*, *128*(4), e2022JG007271. https://doi.org/10.1029/2022JG007271

ThomasArrigo, L. K., Vontobel, S., Notini, L., & Nydegger, T. (2023). Coprecipitation with ferrihydrite inhibits mineralization of glucuronic acid in an anoxic soil. *Environmental Science & Technology*, *57*(25), 9204–9213. https://doi.org/10.1021/acs.est.3c01336

Turetsky, M. R., Abbott, B. W., Jones, M. C., Anthony, K. W., Olefeldt, D., Schuur, E. A. G., et al. (2020). Carbon release through abrupt permafrost thaw. *Nature Geoscience*, *13*(2), 138–143. https://doi.org/10.1038/s41561-019-0526-0

Turetsky, M. R., Treat, C. C., Waldrop, M. P., Waddington, J. M., Harden, J. W., & McGuire, A. D. (2008). Short-term response of methane fluxes and methanogen activity to water table and soil warming manipulations in an Alaskan peatland. *Journal of Geophysical Research*, *113*(G3), 2007JG000496. https://doi.org/10.1029/2007JG000496

Varner, R. K., Crill, P. M., Frolking, S., McCalley, C. K., Burke, S. A., Chanton, J. P., et al. (2022). Permafrost thaw driven changes in hydrology and vegetation cover increase trace gas emissions and climate forcing in Stordalen Mire from 1970 to 2014. *Philosophical transactions. Series A, Mathematical, physical, and engineering sciences*, *380*(2215), 20210022. https://doi.org/10.1098/rsta.2021.0022

Versantvoort, W., Guerrero-Cruz, S., Speth, D. R., Frank, J., Gambelli, L., Cremers, G., et al. (2018). Comparative genomics of Candidatus Methylomirabilis species and description of Ca. Methylomirabilis Lanthanidiphila. *Frontiers in Microbiology*, *9*, 1672. https://doi.org/10.3389/fmicb.2018.01672

Wagner, R., Zona, D., Oechel, W., & Lipson, D. (2017). Microbial community structure and soil p H correspond to methane production in A rctic A laska soils. *Environmental Microbiology*, *19*(8), 3398–3410. https://doi.org/10.1111/1462-2920.13854

Wang, H., Byrne, J. M., Liu, P., Liu, J., Dong, X., & Lu, Y. (2020). Redox cycling of Fe(II) and Fe(III) in magnetite accelerates aceticlastic methanogenesis by *Methanosarcina mazei*. *Environmental Microbiology Reports*, *12*(1), 97–109. https://doi.org/10.1111/1758-2229.12819

Wang, Y., Liu, X., Zhang, X., Dai, G., Wang, Z., & Feng, X. (2022). Evaluating wetland soil carbon stability related to iron transformation during redox oscillations. *Geoderma*, *428*, 116222. https://doi.org/10.1016/j.geoderma.2022.116222

Welte, C. U., Rasigraf, O., Vaksmaa, A., Versantvoort, W., Arshad, A., Op Den Camp, H. J. M., et al. (2016). Nitrate- and nitrite-dependent anaerobic oxidation of methane. *Environmental Microbiology Reports*, *8*(6), 941–955. https://doi.org/10.1111/1758-2229.12487

Williams, A. G. B., & Scherer, M. M. (2004). Spectroscopic evidence for Fe(II)−Fe(III) electron transfer at the iron Oxide−Water interface. *Environmental Science & Technology*, *38*(18), 4782–4790. https://doi.org/10.1021/es049373g

Winkel, M., Mitzscherling, J., Overduin, P. P., Horn, F., Winterfeld, M., Rijkers, R., et al. (2018). Anaerobic methanotrophic communities thrive in deep submarine permafrost. *Scientific Reports*, *8*(1), 1291. https://doi.org/10.1038/s41598-018-19505-9

Woo, M., & Young, K. L. (2006). High Arctic wetlands: Their occurrence, hydrological characteristics and sustainability. *Journal of Hydrology*, *320*(3–4), 432–450. https://doi.org/10.1016/j.jhydrol.2005.07.025

Xiao, L., Wei, W., Luo, M., Xu, H., Feng, D., Yu, J., et al. (2019). A potential contribution of a Fe(III)-rich red clay horizon to methane release: Biogenetic magnetite-mediated methanogenesis. *Catena*, *181*, 104081. https://doi.org/10.1016/j.catena.2019.104081

References From the Supporting Information

Großkopf, R., Janssen, P. H., & Liesack, W. (1998). Diversity and structure of the methanogenic community in anoxic rice paddy soil microcosms as examined by cultivation and direct 16S rRNA gene sequence retrieval. *Applied and Environmental Microbiology*, *64*(3), 960–969. https://doi.org/10.1128/AEM.64.3.960-969.1998

Hales, B. A., Edwards, C., Ritchie, D. A., Hall, G., Pickup, R. W., & Saunders, J. R. (1996). Isolation and identification of methanogen-specific DNA from blanket bog peat by PCR amplification and sequence analysis. *Applied and Environmental Microbiology*, *62*(2), 668–675. https://doi.org/10.1128/aem.62.2.668-675.1996

Holmes, A. J., Costello, A., Lidstrom, M. E., & Murrell, J. C. (1995). Evidence that participate methane monooxygenase and ammonia monooxygenase may be evolutionarily related. *FEMS Microbiology Letters*, *132*(3), 203–208. https://doi.org/10.1111/j.1574-6968.1995.tb07834.x

Muyzer, G., Teske, A., Wirsen, C. O., & Jannasch, H. W. (1995). Phylogenetic relationships ofThiomicrospira species and their identification in deep-sea hydrothermal vent samples by denaturing gradient gel electrophoresis of 16S rDNA fragments. *Archives of Microbiology*, *164*(3), 165–172. https://doi.org/10.1007/BF02529967

Nadkarni, M. A., Martin, F. E., Jacques, N. A., & Hunter, N. (2002). Determination of bacterial load by real-time PCR using a broad-range (universal) probe and primers set. *Microbiology*, *148*(1), 257–266. https://doi.org/10.1099/00221287-148-1-257

Stahl, D., & Amann, R. (1991). Development and application of nucleic acid probes in bacterial systematics. In *Nucleic acid techniques in bacterial systematics* (pp. 205–248). John Wiley & Sons Ltd.

21698961, 2025, 3, Downloaded from https://agupubs.onlinelibrary.wiley.com/doi/10.1029/2024JG008650 by Université de Neuchâtel, Wiley Online Library on [03/02/2026]. See the Terms and Conditions (https://onlinelibrary.wiley.com/terms-and-conditions) on Wiley Online Library for rules of use; OA articles are governed by the applicable Creative Commons License